Searching for rotational and activity signals in M dwarf stars

Author:
Imad Kamil Zayer

Supervised by:
Prof. Hugh Jones
Dr. Mikko Toumi

Centre for Astrophysics Research
School of Physics, Astronomy and Mathematics
University of Hertfordshire

Submitted to the University of Hertfordshire in partial fulfilment of the requirements of the degree of Master's research.

May 2017

Abstract

We search for signals coming from M dwarf stars through variations caused by stellar surface activity.

The aims of this work are to find the stellar rotation period of M dwarf stars and check them against known planetary signals. We used photometric ASAS data for 36 M dwarf stars with literature rotation periods. We used our own noise filtering code and the Systemic Console program to identify the significant signals. In addition, we investigate the correlation between the M dwarf rotation and chromospheric emission, represented by Hα and CaII H&K lines.

This research has provided valuable information regarding how to identify correct stellar rotation periods. We show a good agreement between our photometric rotation periods and corresponding photometric periods in the literature. On the other hand we only find agreement for 8 out of 20 targets where a spectroscopic rotation periods is in the literature. We confirm that several planetary signals of candidate planets reported in the literature are very different to the stellar rotation periods of host stars. For early M dwarfs with periods of less than 40 days we find a relationship between the level of activity as measured by Hα and CaII H&K lines and the photometric rotation period.

Contents

List of Figures

List of Tables

Chapter 1

Introduction

1.1 Introduction

Searching for signals of a planetary system in orbit around nearby stars began in earnest in the 1980s and is described in some detail by (Delfosse et al., 1999). The discovery of the first widely recognized exoplanet by (Mayor, 1995) opened the road to a steadily increasing number of signals that indicate the existence of planets. There are different detection methods used to detect and characterize planetary signals. In the following years, astronomers have improved their hardware and software tools to discover new planets. In general detection methods can be divided into an indirect and a direct method. The planet is usually close to the star and is much less luminous than the star making direct detection of exoplanets extremely difficult. Most confirmed exoplanets have been detected indirectly. There are many different indirect methods, one of these is Doppler spectroscopy or radial velocity (RV) method. It is based on measuring the changes in the radial velocity of the host star as it orbits the common center of mass of the star and its planet. The RV technique is one of the most productive methods to detect exoplanets (Lovis and Fischer, 2010). Variations in radial velocity are caused by variations in the movement of the star towards and away from the Earth. Thus, using this method it is possible to measure these variations in order to confirm if there is a planet orbiting the star. However, the activity-induced radial velocity signals mimic the effect of planets. It is necessary to differentiate between radial velocity signals that correspond to bona fide planets and those that are caused by activity cycles or rotation periods of stars. A method for studying such stellar rotation is to use photometric observations (Kiraga, 2007), where the periodic signals created by brightness variations caused by long-lived spots on the surface of star rotate in and out of view. Therefore we used photometric data to search for photometric counterparts of radial velocity signals.

1.2 M dwarfs stars

M dwarf stars are currently highly attractive targets for exoplanet surveys, they are the most common types of stars in our galaxy, much smaller, cooler and less massive than other on the main sequences. Also, M dwarfs cover 70% of the stars in our galaxy (Covey et al., 2008); (Bochanski et al., 2010). Increasing interest in the study of M dwarfs is due to the fact that it is relatively easier to detect lower mass planets around these types of stars. Such signals may be 20 times larger than velocity variations of the Sun caused by the Earth (10 cm/s) (Omiya et al., 2012).
differentiating between planets and activity-induced signals important at the corresponding periods by using radial velocity and photometry methods.

Many M dwarfs demonstrate intrinsic magnetic activity producing chromospheric and coronal heating, observed in different indicators over the whole stellar spectrum. Since M dwarfs have strong energy outbursts, the classical habitable zones around M dwarfs are unsuitable for the presence of life. However, a large fraction of M dwarfs have limited signs of magnetic activity, and M dwarfs have turned into a prime target for the search for Earth-like exoplanet (Reiners et al., 2012).

Magnetic fields of M dwarfs and solar-type stars produce inhomogeneities on the stellar surface, which represents one noise source in the search for planets via precise radial velocity measurements (Saar and Donahue, 1997).

Magnetic activity impacts spectral lines (Philip, 1985) and generates inhomogeneities in the stellar surface, associated with rotation, which makes Doppler shifts of the stellar spectrum (Saar and Donahue, 1997).

The appearance of Doppler shift from less than one to ten meters per second caused by stellar activity can be induced by changes in the distribution of spots (Huélamo et al., 2008). The resulting signals are probably periodic and they could be a disturbance when searching for planetary signals. This means, that stellar activity is one of the contributors to false positive signals in radial velocity. The ability to distinguish between these signals, which are induced by the stellar activity, from real planetary signals in radial velocity time series curves, is at an early stage in planet-searches. This is what we aspire to study in our current work.

An important effect on radial velocity measurements comes from stellar activity. When activity induces regular modulations in measured radial velocities, these activity signals can be mistaken for planetary signals (Suárez Mascareño et al., 2015). The activity level mainly depends on stellar age for a given spectral type (Kiraga, 2007).

Rotation periods of M dwarfs range from a fraction of a day to up to several hundred days and many of these periods have been discovered only recently (Kiraga, 2007). Stars that have low activity appear to be slow rotators and values of ($v\sin i$) for these stars are below the resolution threshold of roughly 2-3 km/s (Delfosse et al., 1998). One method for measuring rotation periods is by observations of stellar surface inhomogeneities which produce regular modulations during the rotational period (Kiraga, 2007).

M dwarfs undergo a continuous decrease in the level of activity, both chromospheric and coronal as they age (Kiraga, 2007), where the stellar dynamo of weakens with age and active surface areas become much smaller.
Correspondingly, the most active stars seem to rotate rapidly, with rotation periods equal to a fraction of one day and slowing down to several days for low activity stars which seem to rotate slowly (Kiraga, 2007). The stellar projected rotational velocity ($v\sin i$) for these stars are less than the resolution threshold 2-3 km/s (Delfosse et al., 1999). This value of 2-3 km/s corresponding to the lower limit of several days for their rotation periods. Generally, stellar activity is a significant problem for searching stars for exoplanet. Especially, when the stellar rotation periods are close to the orbital period, it is difficult to distinguish between the amplitudes of radial velocities caused by variations of starspots or by planetary variations.

Major factors that affect the activity-related radial velocity noise are the area covered by starspots and plages and the stellar projected rotational velocity ($v\sin i$). Effects of these factors are of the magnitude of the noise. Also, the typical lifetime of active areas, which affect the characterizes of time-scale and temporal behavior (Saar and Donahue, 1997) need to be considered.

1.3 Activity-rotation relation for M dwarfs stars

Across a wide range of the Hertzsprung–Russell diagram, rotation and magnetic activity of stars emerge to be intimately linked. For stars from F to mid-M, it is thought that

coronal and chromospheric emission trace magnetic heating of the stellar atmosphere and are connected with rotation (Delfosse et al., 1999),(Pizzolato et al., 2003).

The broad variety of activity indicators, such as the emission Hα and CaII H&K in the chromosphere tend to grow with increasing rotational velocity until a saturation point is reached and then, activity becomes on the whole insensitive to the rotation (Pallavicini et al., 1981); (Pizzolato et al., 2003). At this saturation point, the threshold rate depends on the stellar mass and emission declines in the most rapid rotators (Browning et al., 2010). Convective inverting of time perhaps limits this threshold (Browning et al., 2010).

Magnetic field generation and subsequent heating in solar-type stars is closely related to stellar rotation, the strength of magnetic heating and surface activity. The effects of angular momentum loss from magnetized winds make rotation slower and as a consequence, decrease magnetic activity with age. These effects produce good evidence for a strong correlation between stellar rotation, magnetic activity and age in solar-type stars. This correlation between activity, rotation and age extends to M dwarfs stars, e.g. (West et al., 2015). We will examine this relation in this work.

Chapter 2

Photometry

2.1 Photometry

Photometry is a technique in astronomy that measures the brightness or flux of electromagnetic radiation of astronomical objects. Photometry compiles light in the telescope and passes it through a filter or the so-called the passband, and then to a photosensitive instrument in order to capture and record the light energy.

According to the widths of passband, photometric systems can be characterized as the following:

- Broadband (passband wider than 30 nm).
- Intermediate band (passband between 10 and 30 nm wide).
- Narrow band (passband less than 10 nm wide).

Photometric measurements can be used to determine the luminosity and distance of an object. This can be accomplished by combining them with the inverse square law in addition to some physical properties of objects, such as chemical composition and temperature, which can be determined by bandwidth and spectrophotometry. Photometric data is used for the study of variable stars (North and James, 2004) and can be beneficial to these measurements to determine the radii of the members of an eclipsing binary star system, the orbital period of planets and rotational periods of stars. The choice for the

V band can be explained by its spectrum and its ability to produce magnitudes that can be seen by a human eye. Apparent magnitude without any further mention usually equates to V-band or visual magnitude (Schulman and Cox, 1997).

2.2 The all-sky automated survey (ASAS)

In on first step of analysing, publicly available photometric data from ASAS was used (Pojmanski, 2002). ASAS is a low-cost project created for photometric monitoring and investigation of all available sky observations (Pojmański, 2004). Presently, ASAS has two observing stations, the southern hemisphere in Las Campanas Observatory, Chile and the other on Haleakala in the Maui island of Hawaii, both of them observing in V and I bands (David et al., 2013). The goal of this survey is to observe stars with varying brightness.

ASAS observations are done with standard Johnson-Cousins V and I filters. Useful data for photometric V-band are taken between the saturation limit $V = 7$ (up to V =8.5 for few frames) and the detection threshold V=14 magnitudes. The smallest aperture MAG_0 is 2 pixels in diameter and is usually best for stars fainter than a V mag of 12. The largest aperture MAG_4 is 6 pixels in diameter and is best aperture for brighter stars than a V mag of 9. For bright stars larger apertures should be used in order to include more photons. For the faint stars, small aperture should be used in order to avoid sky noise.

Optimal aperture choice is dependent upon the magnitude of the target and on the existence of nearby sources (David et al., 2013). The criteria that used to select the aperture is: If $V > 12$ always use MAG_0, if V <9 use MAG_4, otherwise use MAG_X with X=12-V, where V is a mean magnitude. Apertures which have been selected based on this rule have magnitudes exhibiting the lowest standard deviation value. The five apertures MAG_0,...MAG_4 with diameters in the range of 2,3,4,5,6 pixels are equivalent to diameters of circle apertures as the following 30, 45, 60, 75, 90 arecsec respectively.

Sometimes the time series may be unreliable and these criteria may be inappropriate:

- One or more nearby objects are able to affect significantly the signal under considerate.

- When the object imaged is close to the edge of CCD, the image is prone to larger errors. However, this is compensated by having many exposures taken with different pointing (Pojmanski, 2002).
- This data set may have some saturated pixels.

ASAS provides a grade (A - D) for each observation, indicating the quality of that data. We have used only the data from observations with the best quality (grade A) (David et al., 2013).

All of the selected stars for the photometric sample have known rotation periods in the literature.

Chapter 3

Data analysis methods

To detect periodic signals in our data, we used the Lomb-Scargle periodogram. Each target is analysed individually and in the same way as described in the following sections.

3.1 The systemic console

The systemic console program (Meschiari et al., 2009) provides a graphical user interface for fitting and analysing a variety of exoplanetary data with a variety of dynamical analysis tools. Some of the features of this program include interactive fitting of radial velocity time series and transit timing, to get Lomb-Scargle periodograms(Lomb, 1976); (Scargle, 1982)(LSP) with false alarm probability(FAP).

3.2 Periodogram

The time series produced by ASAS are non-uniformly sampled. This is due to changes in the ability to observe the targets of interest for a number of reasons including non-uniform weather conditions, day-time changes, positions of the object under observations in the sky. In this case, the data are not equally spaced, which makes time series analysis very difficult to achieve (Cincotta et al., 1995). Identifying a cycle in such series is impossible with Fast Fourier Transform (FFT) methods because of an irregularly sampled data set (Scargle, 1982). However, FFT has been used on data distributed uniformly which contains full information about all spectral components of the time series (Swan, 1982). An alternative method to FFT is the Lomb-Scargle Periodogram (LSP) (Lomb, 1976);(Scargle, 1982) which is commonly used for calculations of the power spectrum density of unevenly sampled data based on the least squares fit of the sinusoid.

There are many kinds of interpolation that can be obtained to fill in the gaps so they will be evenly spaced. In the case of a radial velocity data set, assume the radial velocity, v, is measured at a time t and N is the number of data points, $v(tj)$, *j=1,2,3....,N0* A Fourier transform for the data set will be:

$$P_v(\omega) = \frac{1}{N}|FT_v(\omega)|^2 \tag{3.1}$$

$$= \frac{1}{N_0}\left|\sum_{j=1}^{N} v(t_j)exp(-i\omega t_j)\right|^2 \tag{3.2}$$

$$= \frac{1}{N_0}\left[\left(\sum_j v_j cos(\omega t_j)\right)^2 + \left(\sum_j v_j sin(\omega t_i)\right)^2\right] \tag{3.3}$$

The equations above compute a basic periodogram for the data set as a function of the frequency ω (Scargle, 1982). Where P is the power, ω is a given period, N is the number of data points for time series,v is the radial velocity measured at a time t. If the data set displays a sinusoidal pattern with a frequency of (ω_0) , then *v(t)* and *exp(-ω_t)* in the phase and this leads to a sinusoidal signal near ω giving a major contribution to the sums in the equation. At other values of ω that are far from a real sinusoidal signal in the sum will randomly oscillate between positive and negative and the results more or less cancel yielding a small sum. Therefore, if a sinusoidal signal of period (ω) is present in the data set, the value of $P_v(\omega)$ will be large (Scargle, 1982). With the periodogram, we can locate our search to a defined set of frequencies. Since $P(-\omega)$ $=P(\omega)$, a proximately, half of the information in the data is omitted when calculating the periodogram, the absolute value part of the equation does not discriminate between the negative and positive frequencies. Therefore, we will only look at *(N=N0/2)*, evenly spaced frequencies.

3.3 False alarm probability (FAP)

The false alarm probability (FAP) is the probability of finding a spurious peak in a light curve for a given power (Horne and Baliunas, 1986). Powers which have a low FAP are unlikely to have random peaks. In our periodogram FAP has the following equation:

$$FAP = 1 - (1 - e^p)^n \tag{3.4}$$

Where p is the power of the highest peak, and n is the number of independent frequencies in the frequency range of interest(Sturrock and Scargle, 2010).
The three horizontal dashed lines in the periodogram indicate 0.01%, 0.001% , 0.0001%

FAP. We consider peaks higher than 0.01% to be statistically significant (0.01% probability that the signal arises from noise), and that means these peaks have a confidence level of 99.99%. The significance of power is increased with lower levels of noise and/or more data points.

3.4 Detection of aliasing frequencies

Differentiating an alias frequency from a physical one is a common problem. Those making the correct diagnosis is crucial for identifying the correct frequency. Aliases are caused by discretely sampling continuous signals. The discretely-sampled signal arises from the continuous signal and the sampling function, where there is a convolution between the periodogram of the continuous signal and the periodogram of the sampling function.
In fact, the stellar observations are done only at night when the star is high enough in the sky to observe, so daily and yearly gaps in observations create a daily and yearly alias. There are 12 hours (on average) between each data point. Therefore a curve with a period of 24 hours can be made to fit the data (Dawson and Fabrycky, 2010).

To detect the alias periods in the periodogram and the periodogram of the window function, we consider that the alias frequency is f_s and the physical frequency is f_a, the alias formula will be $f_s \pm n f_a$, where n is an integer. Since period (p) is 1/f, then the alias formula becomes $1/(1/p_s \pm 1/p_a)$ and the result of this formula is two alias periods.

The steps of the detection of alias peaks are as follows :

- Plot the window function, we usually see peaks at a periods of one day, one year, one solar day, one sidereal day. If observations were taken over a specific part of the lunar cycle, then we see peaks at one month, one month± one year.

- Plot the periodogram and consider first the probability that the largest peak occurs at a physical period p_s.

- Consider that each peak in the window function occur at alias period p_a and then use the alias formula, to find the expected periods (see chapter 3).

- Consider that largest peak in periodogram is p_s and other peaks are p_a and apply the formula.

- Consider the largest peak in the window function is a physical period p_s and that each peak in the periodogram occurs at alias periods p_a and then use alias formula.

- Matching all the resulting alias periods with the periods in periodogram, if there is a coincidence between them, then that means these periods are alias periods.

3.5 Data Analysis

In this section, we described the stages that we follow in analysing of our sample taking GJ382 as an example. Our goal of this section at first, how to detect the outliers and determining whether a period in periodogram is correct or just alias. In the (3.5.1), (3.5.2) subsections, we will describe how our code removed the outliers from raw data. We will show which points have been removed and how. In section (3.5.3), we will present how we choose the proper aperture. In section (3.5.4), we will describe the analysing of periodogram of residual by using a particular example. In section (3.5.5), we will analyse the window function for the same target and distinguish between physical signals and aliases signals, and in section (3.5.6) we check whether the phase-folded data corresponds to the stellar rotation period.

3.5.1 Removing outliers from data

We remove outliers from data by detecting points that are more than five times standard deviation (5σ) away from the mean value. Choosing a value of the standard deviation depends on the number of outliers in the data. In this work we investigated (3σ) and (5σ), if there is a 3σ outlier, the chances of it not being an outlier are 0.3% given a Gaussian probability distribution of the data, while for 5σ the probability is less than 0.0001.
This method involves weighting the data points based on the assumption that the data are Gaussian distributed. The aim of using it is to reduce the effect of non-normal outliers in data. The identification of outliers in data points does not mean we have bad data. This means they do not agree with Gaussian noise.

3.5.2 Comparison between raw and clean data

Outlier data can be removed using our code with difference sigma threshold. The threshold depends on the signal to noise ratio (S/N)= P_{signal} /P_{noise}= μ/σ, where μ is mean or expected value, σ is the standard deviation of the noise. For identifying how many data points removed from the raw data we compare between the number of data points (N) and the standard deviation (STD) values of them in Tables(3.1&3.2). The number of data points available for our objects always exceeded 300 data points.

From Tables(3.1 &3.2) and Figure(3.1), it can see how many outlying data points have been removed. For GJ382 as an example, we using MAG_3 in our analysis. For raw data (N=439; STD=22.57) and for clean data(N=437; STD=20.80), we find that 2 points were rejected using a 5σ threshold and we used the 437 remaining measurements in our fitting see Figure(3.1), the periodogram changes. In general, the number of points which we rejected is typical 1-2%.

Figure(3.2) illustrates that the distribution of data points can deviate from the assumed Gaussian distribution as outliers are detected based on the value of σ. Removing outliers restricts outlying data points to have a strong impact on periodograms and inferences made from them and that may change for different candidate periods, as the prior also changes.

TABLE 3.1: Raw data of GJ382. MAG is aperture, N is number of data points, Mean is mean of magnitude in each aperture, STD is the standard deviation of the mean value.

MAG	N	Mean(mag)	STD(mmag)
0	437	9.238	45.69
1	438	9.243	32.94
2	438	9.242	25.77
3	439	9.246	22.57
4	439	9.244	23.65

TABLE 3.2: Characteristics of cleaned data for GJ382. Mean is the mean of the magnitude in each aperture, STD is the standard deviation of the mean value.

MAG	N	Mean(mag)	STD(mmag)
0	435	9.241	35.85
1	435	9.244	28.19
2	436	9.243	22.42
3	437	9.247	20.80
4	437	9.245	21.76

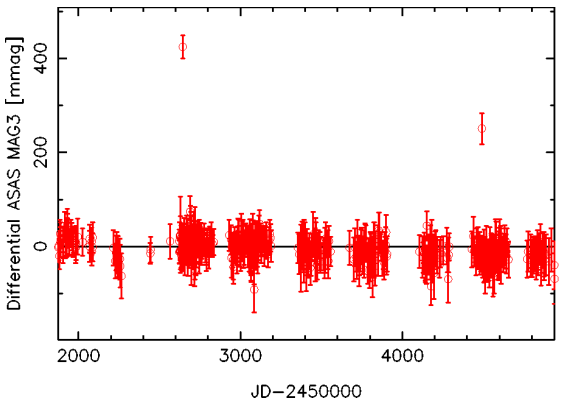

(A)

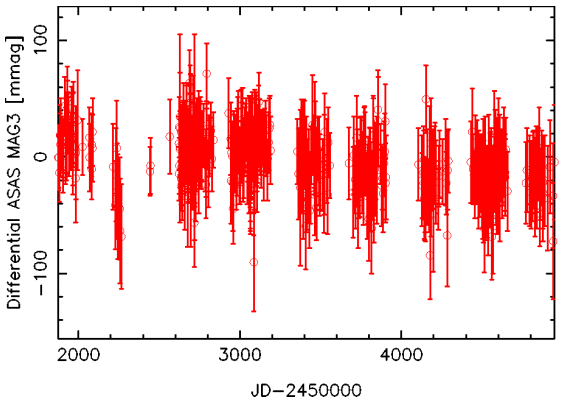

(B)

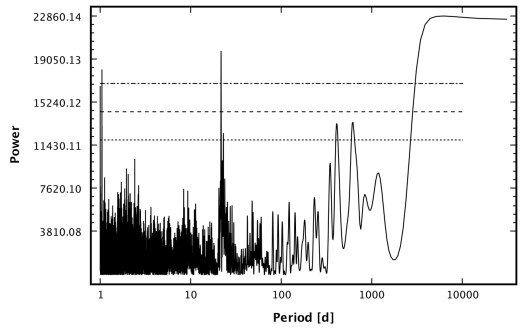

(C)

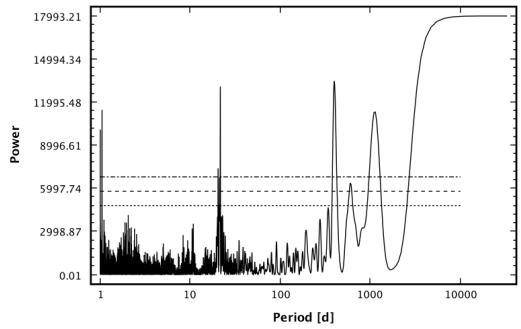

(D)

FIGURE 3.1: (A)Raw data for GJ382, (B)Data after removing outliers, (C) Periodogram of raw data, (D)Periodogram of cleaned data. Note that removing outliers makes periodogram peaks more significant.

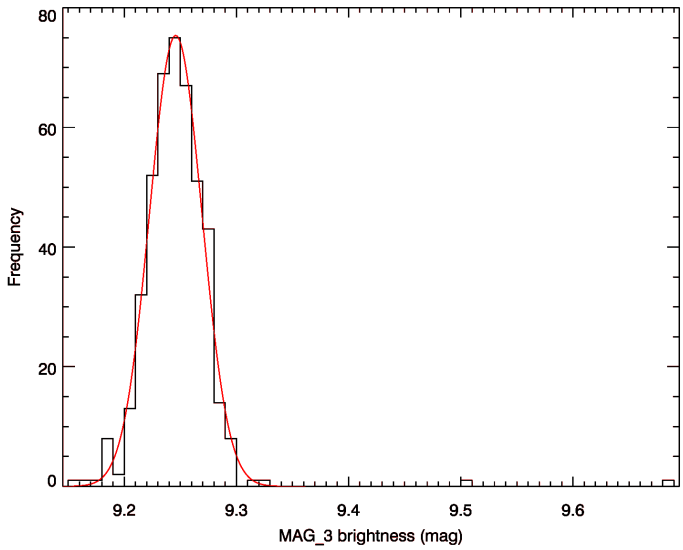

(A)

FIGURE 3.2: Gaussian distribution of data points included in periodogram. The red fit line shows the outliers removed at more than 5σ for GJ382 using aperture MAG_3

3.5.3 Comparison of apertures

The optimal aperture which must be chosen in our analyses depends on the magnitude of the target and whether the target has a companion. We choose the aperture before starting with our analysis. We examined if there is a companion or a star in the background of that particular target. We also wanted to make sure we used the best aperture size in our analysis for all our targets and the chosen apertures have no companions with in them.
Existence of a companion close to our target may cause blending in the data and that the magnitude to deviate from the true value for the target of interest.

For example, GJ877 is one of M dwarfs observed in the V-band and it has magnitude V=10.37 mag, whilst its companion has V=10.43 mag, therefore the interpretation of signals in periodogram is problematic see Table (4.2) and periodogram(35) in Figure(4.2).

GJ382 was taken as example, for this target we have chosen MAG_3 (5 pixels) which is equivalent to 75 arcseconds in the field of view. There was no evidence for the existence of a companion to our target in this area. The near of companion distance is 87.21

arcseconds.

The standard deviation of ASAS magnitudes was checked against the different apertures, see Tables(3.1&3.2), We can see the two apertures have a standard deviation of 20.80 mmag and 21.76 mmag in MAG_3 and MAG_4, respectively. They exhibit similar variability, whilst the MAG_0 has the highest standard deviation(35.85 mmag) among other apertures, therefore we should use MAG_3. This choice is also consistent with the criterion laid out in section (2.2). Also, we use MAG_4 to ensure the results are correct because it is expected to get similar results, see Figure (3.3). Therefore, we look at the differences between MAG_0, MAG_3 and MAG_4, we can see the FAP in MAG_0 is higher than MAG_3 and MAG_4. Thus using the MAG_3 and MAG_4 is the best choice for this target and consistent with our criteria in section(2.2).

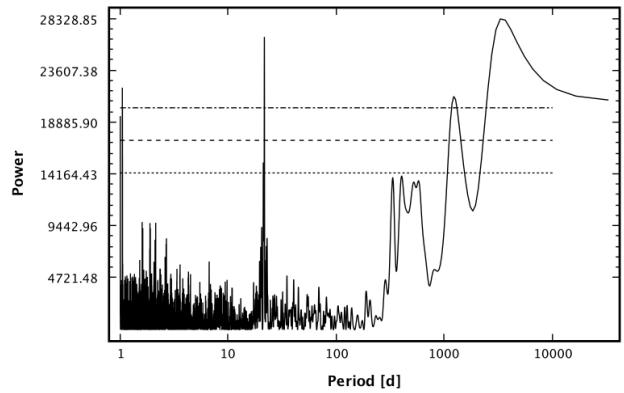

(A)

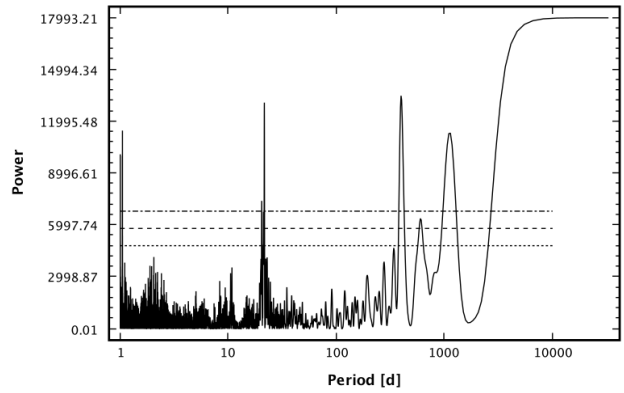

(B)

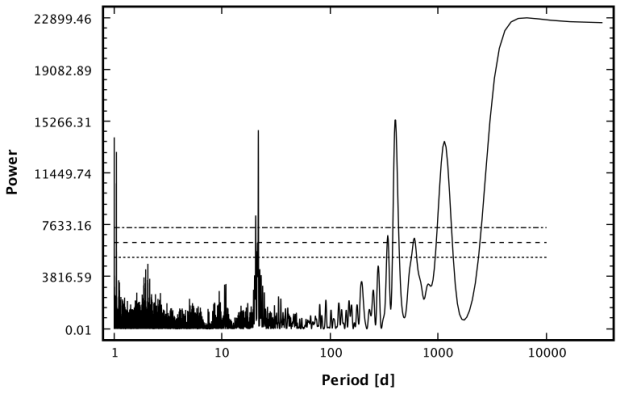

(C)

FIGURE 3.3: Lomb-Scargle periodogram of the ASAS photometry of GJ382:(A)MAG_0 (B) MAG_3; (C) MAG_4, where the MAG_3 and MAG_4 are similar, while MAG_0 has higher standard deviation. The three horizontal dashed lines in periodogram indicate 0.01%, 0.001%, 0.0001% false alarm probability(FAP).

ASAS photometric data provides a type of standard deviation (uncertainty) estimate for all of the apertures. We display in figure (3.4) the distribution of uncertainties for selected magnitudes by the formula in section (2.2), to select the best aperture for each target.

Figure(3.4) illustrates the distribution between ASAS magnitudes of the targets in this work with their uncertainties, where there is increase in uncertainty when going from 8

to 12th mag for the sample of this work. We use linear regression to show how decreasing uncertainties are associated with decreasing magnitudes. There are two targets showing high uncertainties, GJ667C has 524 mmag uncertainties because it has a companion. GJ1057 has 211 mmag uncertainties, presumably due to an unseen companion or high activity. Thus, analysing these two targets is subject to a high degree of uncertainty.

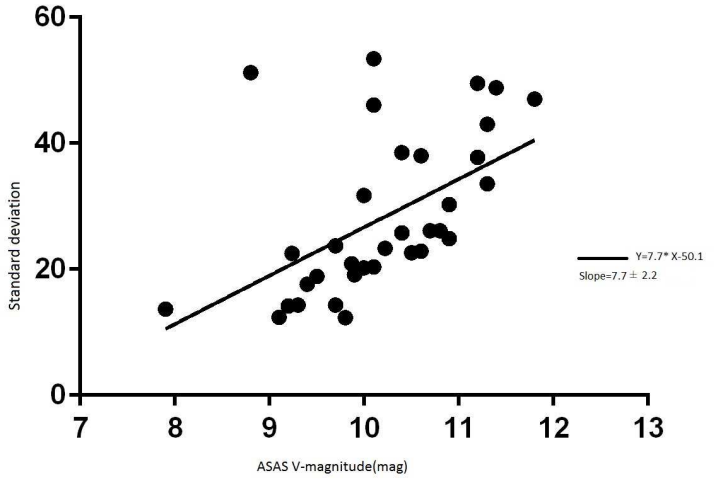

FIGURE 3.4: Distribution of the standard deviations (uncertainties) for ASAS magnitudes of each target in our sample, we show decreasing standard deviation with increasing magnitude. The black line represents a linear regression to fit the relationship between ASAS magnitude and their standard deviation, with the equation; y= 7.7x –50.1 and slope= 7.7±2.2

3.5.4 Analysis of residual periodogram

In order to obtain the most accurate estimate of the rotation period possible, we fit and subtract the signal of any long-term trend from the original data. We did this procedure by using the residual periodogram.

In Figure(3.5), the periodogram (A)for GJ382 shows significant peaks near 1 day, 21.54 days, 396.3 days 1133.4 days and 32900 days. We see a very long term trend at 32900 days due to a slope in the data and it is over the time span of the observation. Including this period of long-term trend in the model decreases the $\tilde{\chi}^2$ value from 0.54 to 0.1($\tilde{\chi}^2$ is an indicator of the agreement between the observed and expected distribution of data points. A decreasing$\tilde{\chi}^2$ value, shows a better agreement). This procedure corresponds to removing a linear trend from the data. We should remove large-amplitude variations or long-term trends, in order to find the stellar rotation signals more clearly.

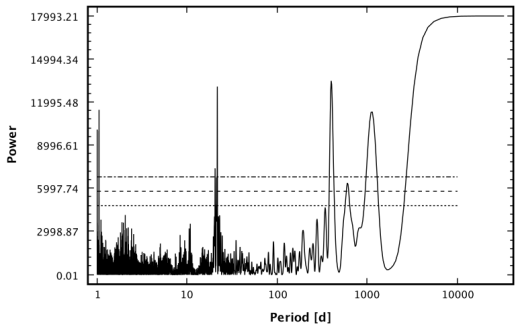

(A)

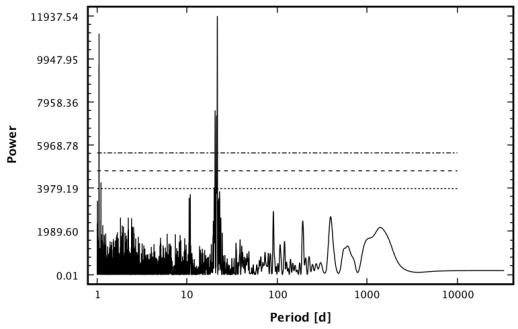

(B)

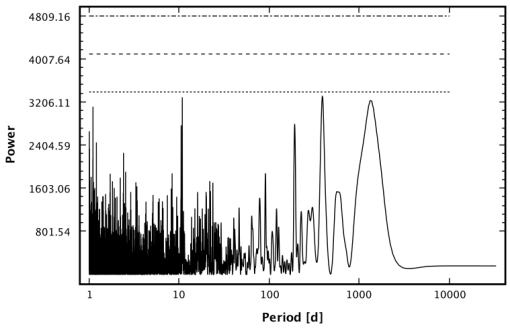

(C)

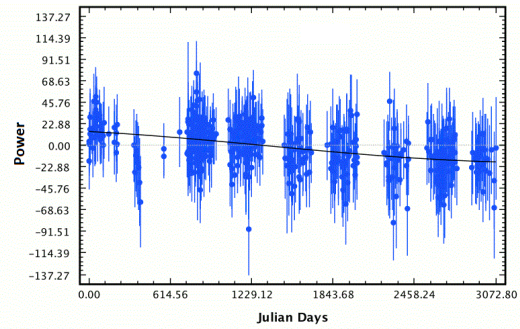

(D)

FIGURE 3.5: (A) Generalized Lomb-Scargle periodogram of original data for GJ382, while (B) residual periodogram after subtracting a sinusoid fit to the long period magnetic activity(removing a linear trend from the original data), (C) second residual periodogram after subtracting 21.54 day rotation periods. The three horizontal dashed lines in periodogram indicate 0.01%, 0.001%, 0.0001% false alarm probability from bottom to top, (D)data points after subtracting a sinusoid fit to long period trend.

After subtracting the long-term trend from the data, we then carefully examined the periodogram of the residuals to see what peak is removed or decreased, see Figure(3.5B). The peaks at 396.3 days(it is close to one year alias) and 1134 days disappeared when the primary peak was removed, as these peaks are linked to the long period trend and not independent, they are each other's yearly aliases. We reject peaks near one year as aliases produced by observing cadence, as we show in the next section. Now, we see two noteworthy things. First, we see that the peak at around 1- day remains and it is a short period, it can be affected by daily aliasing of the dominant power at 21.54 days, as discussed in the next section.

Second, the periodicity at 21.54 days also remains, there are few peaks in close range periods because it is probably that differential spot rotation produces periodicities near the prime period.

We repeated the first procedure but with the peak at 21.54 days, we may run up a periodogram of the residuals and see what is left in the data see Figure (3.5 B,C). There is no any significant peak up to the level of FAP, that means there is not anything else important.

3.5.5 Analysis of window function

The photometric observation of stellar periods and variations are suffering from an alias problem. In this section, we will describe how to distinguish between physical and spurious (alias) periodicities by taking the GJ382 as an example.

We will start with analysis of the window function(or periodogram of time sampling) for GJ382 as shown in Figure (3.6).

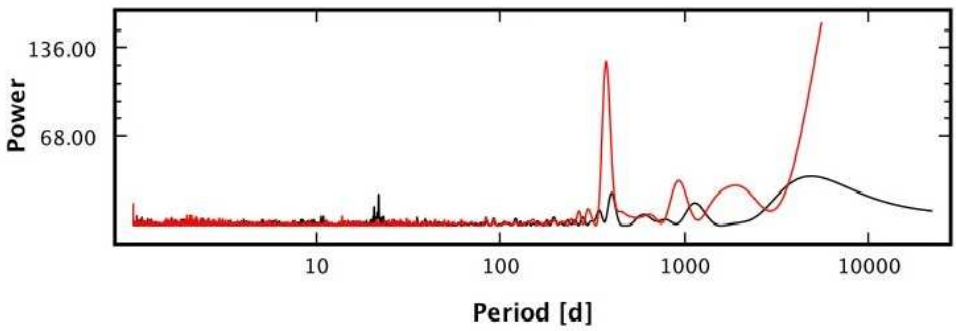

FIGURE 3.6: Window function with Periodogram of GJ382. We indicate the periodogram of the original time series by the black line, and the red line indicates window function near one year, more than 4806 days, as well 365, 918, 1865 and near 1 days (there are no real observations at these intervals). We note these peaks can be a source of spurious (alias) periodicities, they occur at nf_s, where n is an integer.

We can see there are significant peaks in both the window function and the periodogram. We used the alias formula $= 1/(1/p_s \pm 1/p_a)$ to distinguish between real and unreal peaks or aliases peaks.
The red peaks in the window function are as the following: peak at more than 4806 days, as well 365, 918, 1865 and near 1 day. The black peaks are 4806, 397, 21.54, near 1 days.
The significant peaks in periodogram are as the following, 4806, 1134, 396, 1.04 days and are illustrated in the top panel of Figure 3.5

We considered the high peak in periodogram at 32900 days is a real a peak and the red peaks in window function are aliases peaks. Using the alias formula, we found there are aliases peaks in the window function at 356, 374, 1764 and 944 days.

Now consider that the peak at 4806 days is a real peak and others in the window function are aliases peaks. Using the alias formula, we found aliases peaks at 356, 1134 and 401 days.

By the same procedure, consider that the peak at 21.54 days in periodogram is real and the others are aliases, we found that the peak at 1.04 day is a daily alias of the peak at 21.54 days.

We calculated the window function, we can show clearly that peaks in window function are linked to more in the periodogram: 356, 918 (near 944 days), 1895 (near 1764 days), 397 (near 401), near 1 day and 1134 days. All of these peaks are unreal and just yearly aliases of high activity cycle peaks or aliases of yearly alias peaks. On the other hand, we can see that peaks at 4806.6 and 21.54 are real.
By the same process, for significant peaks in periodogram, we see that peaks at 396 (near 401) and 1134 days are yearly aliases of activity cycle, 32900 days is extension of the cycle at 4806 days(there are no real observations at this interval), and 21.54 is a real peak.

Finally, we conclude that peak 21.54 days is a possible rotation period, the peak at more than 4806 days is the activity cycle, 1134 and 396 are yearly aliases of the activity cycle and 1.04 days is the daily alias of the rotation period.

3.5.6 Analysis of phase-folding

To further check for and to show strong evidence for the possible rotation periods found by our analyses, we checked the phase-folded light curve of our targets and take the rotation period of GJ382 as an example in this section.
In Figure (3.7A), we show the shape of the period 21.54 days of stellar rotation. In Figure(3.7B), we show the phase-folded of this period. We divided the period 21.54 days into five intervals. We can see there is a clear period at 21.54 days, thus we can confirm that this period is induced from stellar rotation period and that there is no other phenomena, such as the eclipse of a binary star that needs to be considered.

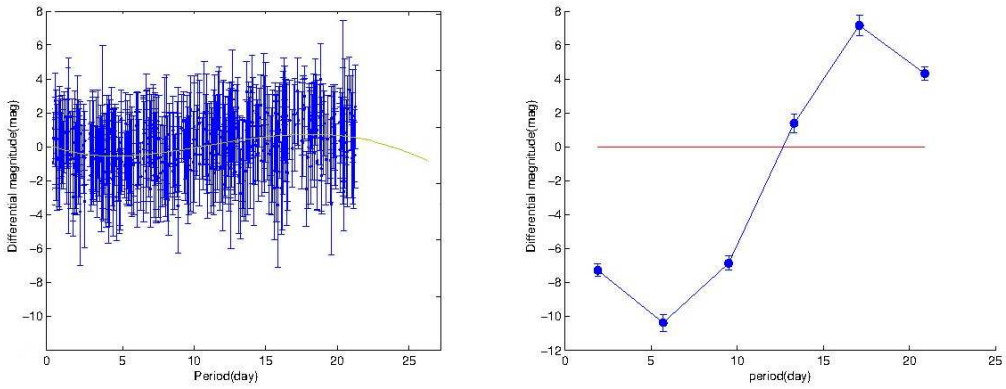

(A) (B)

FIGURE 3.7: (A) is folding of the data to the rotation period 21.54 days identified in the periodogram with the best-fit sinusoidal. (B) is the phase folded points of rotation period 21.54 day after binning the data, the red line is a weighted mean of the data points in this period. We note the expected form of a light curve with a 21.54 days period is appearing.

Chapter 4

Results and Discussion

Our sample consists of 36 M dwarfs stars with ASAS photometric data, and visual magnitudes V in the range 8-14 mag.

The present work is focussed on analysing of M-type stars with known rotation periods. Particular attention has been taken to investigate time series variations and identifying the rotation periods of stars, comparing with literature, investigating planetary signals and rotation activity relation.

Information has been provided on the spectral type, apparent magnitude, radius, planetary periods of some planets as shown in Table(4.1). Interpretation of the identified signals, their false alarm probability, periodograms and values of photometric or spectroscopic rotation periods for each target from the literature, are given in Table (4.2) and Figures(4.2-4.5).

TABLE 4.1: Stellar parameters for our sample of M dwarfs: (Seq) is sequence of targets and it is same in Tables (4.2-4.5) and Figure(4.1). (ST) spectral type, (V) magnitude,(MAG) photometric aperture, (STD) standard deviation, R*($R_{\odot}$) stellar radius in units of solar radius from (1) (Houdebine et al., 2016) and (2) (Kiraga, 2007).

Seq.	Target	ST	V (mag)	MAG	STD(mmag)	R*($R_{\odot}$)
1	GJ103	M0	8.85	3	51.2	-
2	GJ84	M2.5	10	2	20.2	-
3	GJ3367	M0	10.9	1	30.3	-
4	GJ375	M3.5	11.37	1	33.6	-
5	GJ431	M3.5	11.5	0	770.6	0.386 ± 0.046
6	GJ669A	M3.5	11.33	1	43	-
7	GJ729	M3.5	10.49	1	25.8	0.197 ± 0.018
8	GJ285	M4	11.2	1	49.5	0.359 ± 0.042
9	GJ182	M0	10.1	2	53.4	-
10	GJ494	M0.5	9.7	2	23.7	-
11	GJ3331	M1.5	10.4	2	38.5	-
12	GJ9520	M1.5	10	2	31.7	-
13	GJ2036A	M2	10.7	1	26.1	-
14	GJ569A	M2	10.1	2	46.1	-
15	GJ551	M6	11.22	1	37.8	-
16	GJ205	M1.5	7.9	4	13.7	0.643 ± 0.052
17	GJ382	M1.5	9.24	3	22.5	0.544 ± 0.51
18	GJ536	M1	9.7	2	14.3	0.519 ± 0.047
19	GJ876	M3	10.1	2	20.4	-
20	GJ358	M2	10.6	1	38	0.425 ± 0.041
21	GJ176	M2	9.9	2	19.1	-
22	GJ674	M3	9.4	3	17.6	0.357 ± 0.031
23	GJ676A	M0	9.5	2	18.9	-
24	GJ433	M2	9.88	2	12.3	0.465 ± 0.041
25	GJ273	M3	9.87	2	20.9	0.32 ± 0.029
26	GJ701	M2	9.3	3	14.4	0.463 ± 0.040
27	GJ581	M4	10.5	1	18.2	-
28	GJ436	M1	10.61	1	22.9	0.458 ± 0.055
29	GJ846	M1	9.14	3	12.4	-
30	GJ588	M2	9.31	3	14.3	0.484 ± 0.047
31	GJ163	M3.5	11.81	0	47	0.439 ± 0.09
32	GJ357	M3	10.9	1	24.9	0.333 ± 0.32
33	GJ832	M2	9.2	3	14.2	-
34	GJ1057	M5	14	0	211	-
35	GJ877	M2	10.3	2	22.6	-
36	GJ667c	M3	10.2	2	524	-

4.1 Period Search

A search for stellar rotation by using the photometrically derived rotation of periodic signals of long-lived spots on the stellar surface that rotate in and out of view. Out of 36 analysed stars, only 26 showed statistically significant periodic variations as indicated in the Tables (4.2-4.5):

TABLE 4.2: Periods obtained from this work with their uncertainties, false alarm probability (FAP) and interpretation for each period. (AC) represents activity cycle of star, P_{rot} is rotation periods by this work. These P_{rot} are compared with literature. $P_{\rm phot}$ represents photometric rotation period from literature, $P_{\rm sp}$ is spectroscopic rotation period from literature. Order of targets as the following: Targets in sequence of 1-14 have P_{rot} by this work and compared with $P_{\rm phot}$, targets for 15-23 have P_{rot} by this work and compared with $P_{\rm phot}$ and $P_{\rm sp}$, targets 24-34 have no evidence for P_{rot} by this work and they just have $P_{\rm phot}$ and $P_{\rm sp}$, finally targets 35-36 not valid to analysing, we could not interprete them, they just have $P_{\rm sp}$. The references of $P_{\rm phot}$ and $P_{\rm sp}$ as the following: (1) represents(Kiraga, 2007); (2) (Suárez Mascareño et al., 2015) ; (3) (Irwin et al., 2011); (4) (Robertson et al., 2014); (5) (Benedic et al. 1998) (6) (Nelson et al., 2016); (Robertson et al., 2015) ; (7) (Collins et al., 2016)

.

Seq.	Target	P(day)	FAP	Interpretation	$P_{\rm phot}$(day)	$P_{\rm sp}$(day)
1	GJ103	4632 ± 3300	1.27×10^{-30}	AC	1.563(1)	-
		1.0003 ± 0.0009	1.72×10^{-14}	daily alias of AC		
		1621 ± 58	3.02×10^{-11}	yearly alias of AC		
		341 ± 3	1.4×10^{-8}	yearly alias of AC		
		1.561 ± 0.003	3.89×10^{-15}	P_{rot}		
		2.758 ± 0.003	1.072×10^{-9}	daily alias of P_{rot}		
2	GJ84	43.107 ± 0.095	2.68×10^{-4}	P_{rot}	44.51(1)	-
3	GJ3367	12.05 ± 0.07	9.38×10^{-5}	P_{rot}	12.05(1)	-
4	GJ375	1.879 ± 0.005	1.54×10^{-1}	P_{rot}	1.877(1)	-
5	GJ431	14.33 ± 4.04	6.63×10^{-11}	P_{rot}	14.3(1)	-
		1.071 ± 0.008	7.59×10^{-11}	daily alias of P_{rot}		
6	GJ669A	2789 ± 150	1.54×10^{-10}	AC	0.9(1)	-
		421 ± 5	7.7×10^{-5}	yearly alias of AC		
		338 ± 2	2.01×10^{-4}	yearly alias of AC		
		1.0492 ± 0.0001	7.46×10^{-4}	P_{rot}		
7	GJ729	750 ± 12	3.36×10^{-9}	AC	2.9(1)	-
		242 ± 75	4.84×10^{-5}	yearly alias of AC		
		2.865 ± 0.009	8.76×10^{-8}	P_{rot}		
		1.543 ± 0.004	4.87×10^{-6}	daily alias of P_{rot}		
8	GJ285	3979 ± 550	4.577×10^{-26}	AC	95(3)	
		1.0003 ± 0.0002	1.58×10^{-19}	daily alias of AC		
		328.1 ± 2.8	7.05×10^{-13}	yearly alias of AC		
		2.701 ± 0.004	8.89×10^{-7}	P_{rot}		
		1.501 ± 0.003	2×10^{-5}	daily alias of P_{rot}		
9	GJ182	2916 ± 321	1.79×10^{-22}	AC	4.4(1)	-
		4.4 ± 0.02	4.66×10^{-14}	P_{rot}		
		1.294 ± 0.003	$1.1.24 \times 10^{-13}$	daily alias of P_{rot}		
		4.421 ± 0.017	1.30×10^{-13}	daily alias of P_{rot}		

TABLE 4.3: Continued

Seq.	Target	P(day)	FAP	Interpretation	$P_{\rm phot}$(day)	$P_{\rm sp}$(day)
10	GJ494	1392 ± 36	6.83×10^{-8}	AC	2.9(1)	-
		2.881 ± 0.004	5.92×10^{-17}	P_{rot}		
		1.532 ± 0.002	2.90×10^{-13}	daily alias of P_{rot}		
		1.524 ± 0.003	4.29×10^{-12}	daily alias of P_{rot}		
11	GJ3331	3609 ± 110	6.64×10^{-59}	AC	0.3(1)	-
		1.0003 ± 0.0003	1.23×10^{-35}	daily alias of AC		
		321.6 ± 1.8	1.26×10^{-23}	yearly alias of AC		
		663 ± 930	1.84×10^{-14}	yearly alias of AC		
12	GJ9520	2438 ± 980	5.42×10^{-10}	AC	0.4 (1)	-
		1.0005 ± 0.0001	5.99×10^{-7}	daily alias of AC		
		309 ± 4	2.56×10^{-5}	yearly alias of AC		
		665.1 ± 6.1	1.18×10^{-2}	yearly alias of AC		
13	GJ2036A	2.981 ± 0.008	1.64×10^{-4}	P_{rot}	0.8(2)	-
		2.97 ± 0.03	6.5×10^{-4}	daily alias of P_{rot}		
		1.49 ± 0.06	1.13×10^{-2}	daily alias of P_{rot}		
14	GJ569A	3947 ± 290	2.57×10^{-45}	AC	13.7	-
		408.4 ± 2.4	7.43×10^{-26}	yearly alias of AC		
		333.6 ± 5.7	1.34×10^{-17}	yearly alias of AC		
		1184 ± 21	4.24×10^{-16}	yearly alias of AC		
		13.60 ± 0.06	4.74×10^{-1}	P_{rot}		
		1.0003 ± 0.0006	3.43×10^{-29}	daily alias of P_{rot}		
		1.0008 ± 0.0045	1.86×10^{-7}	daily of alias of P_{rot}		
15	GJ551	1872.953 ± 0.005	1.4×10^{-7}	AC	82.53(1)	82.6(7)
		1.0095 ± 0.0002	6.97×10^{-10}	daily alias of AC		
		247.891 ± 0.002	189×10^{-7}	yearly alias of AC		
		106.01 ± 7.32	1.53×10^{-4}	yearly alias of AC		
		83.03 ± 0.02	1.85×10^{-12}	P_{rot}		
16	GJ205	1292 ± 58	8.49×10^{-9}	AC	33.61(1)	35(2)
		1.025 ± 0.001	1.21×10^{-7}	daily alias of AC		
		33.54 ± 0.15	3.6×10^{-5}	P_{rot}		
		36.970 ± 0.105	5.33×10^{-6}	Differential P_{rot}		

Table 4.4: Continued

Seq.	Target	P(day)	FAP	Interpretation	$P_{\rm phot}$(day)	$P_{\rm sp}$(day)
17	GJ382	32900 ± 470	6.44×10^{-15}	AC	21.56(1)	21.7(2)
		1134 ± 46	3.04×10^{-8}	yearly alias of AC		
		396 ± 16	2.08×10^{-10}	yearly alias of AC		
		21.54 ± 0.02	1.11×10^{-3}	P_{rot}		
		1.041 ± 0.005	2.17×10^{-8}	daily alias of P_{rot}		
18	GJ536	43.3 ± 0.1	1.29×10^{-3}	P_{rot}	-	43.8(2)
		1.021 ± 0.003	2.89×10^{-3}	daily alias of P_{rot}		
19	GJ876	1786 ± 23	1.38×10^{-3}	AC	95.0(6)	87.3(2)
		81.19 ± 0.02	2.04×10^{-3}	P_{rot}		
		1.0091 ± 0.0001	4.12×10^{-4}	daily alias of P_{rot}		
		2.642 ± 0.006	2×10^{-2}	daily alias of P_{rot}		
20	GJ358	6526 ± 7100	1.31×10^{-71}	AC	25.26(1)	16.9(2)
		604 ± 27	5.54×10^{-19}	yearly alias of AC		
		1631 ± 32	8.78×10^{-18}	yearly alias of AC		
		343 ± 2	4.06×10^{-12}	yearly alias of AC		
		25.23 ± 0.03	8.63×10^{-10}	P_{rot}		
		1.0002 ± 0.0003	1.77×10^{-41}	daily alias of P_{rot}		
21	GJ176	40.87 ± 0.21	6.18×10^{-5}	P_{rot}	39.5(7)	39.3 (2)
		1.02 ± 0.02	3.03×10^{-4}	daily alias of P_{rot}		
22	GJ674	3523 ± 820	1.10×10^{-34}	AC	33.3(1)	32.9(2)
		337 ± 3	3.65×10^{-6}	yearly alias of AC		
		411.8 ± 3.5	2.37×10^{-5}	yearly alias of AC		
		35.03 ± 0.01	0.22×10^{-3}	P_{rot}		
		1.0003 ± 0.0004	1.95×10^{-20}	daily alias of P_{rot}		
23	GJ676A	3177 ± 170	4.25×10^{-21}	AC	-	41.2(2)
		1.0004 ± 0.0004	8.31×10^{-18}	daily alias of AC		
		327.6 ± 2.6	3.74×10^{-11}	yearly alias of AC		
		32.04 ± 0.11	3.82×10^{-2}	P_{rot}		
24	GJ433	-	-	-	-	73.2(2)
25	GJ273	-	-	-	-	115(2)
26	GJ701	-	-	-	-	127.8(2)
27	GJ581	-	-	-	130(4)	132(2)
28	GJ436	-	-	-	-	39.9(2)

Table 4.5: Continued

Seq.	Target	P(day)	FAP	Interpretation	$P_{\rm phot}$(day)	$P_{\rm sp}$(day)
29	GJ846	-	-	-	-	31 (2)
30	GJ588	-	-	-	-	61.3(2)
31	GJ163	-	-	-	-	61(2)
32	GJ357	-	-	-	-	74.3(2)
33	GJ832	5355 ± 290	3.2×10^{-3}	AC	-	45.7(2)
		1.0003 ± 0.0002	3.85×10^{-5}	daily alias of AC		
		714 ± 170	3.8×10^{-2}	yearly alias of AC		
34	GJ1057	-	-	-	102(3)	-
35	GJ877	52.75 ± 0.06	1.19×10^{-12}	-	-	116(2)
		54.49 ± 1.05	1.72×10^{-6}			
		1.0151 ± 0.0005	9.02×10^{-6}			
		503.8 ± 5.6	1.57×10^{-4}			
36	GJ667C	-	-	-	-	103.9(2)

FIGURE 4.1: Generalized Lomb-Scargle periodograms for the ASAS photometry of our sample.The three horizontal dashed lines in periodogram indicate 0.01%, 0.001% and 0.0001% FAP. Order of targets as the following: Targets in sequence of 1-14 have P_{rot} by this work and photometric P_{rot} from literature , targets for 15-23 have P_{rot} by this work as well photometric and spectroscopic P_{rot} from literature, targets 24-34 have no evidence for P_{rot} by this work and they just have photometric and spectroscopic P_{rot} from literature, finally targets 35-36 not valid, we could not interpreted them, they just have $P_{\rm sp}$.

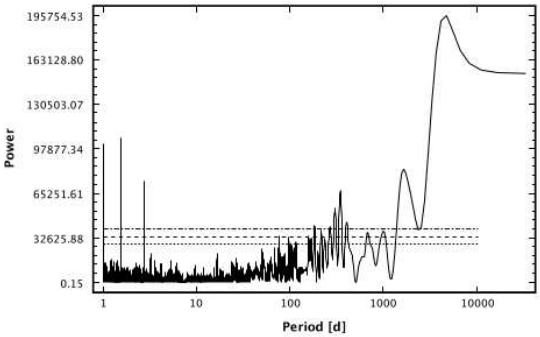

(1) GJ103

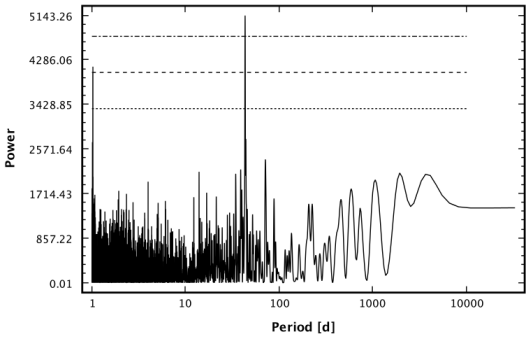

(2) GJ84

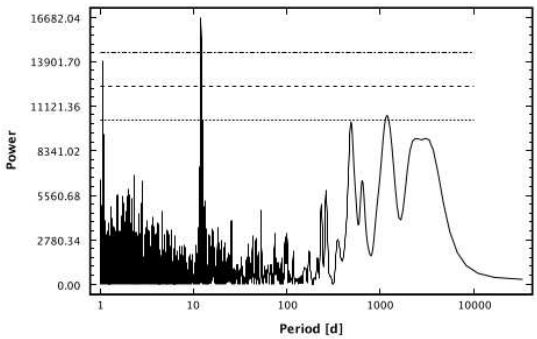

(3) GJ3367

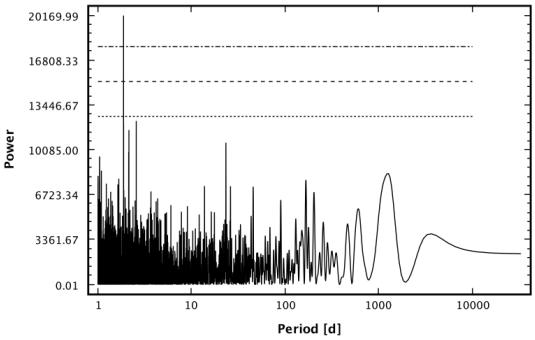

(4) GJ375

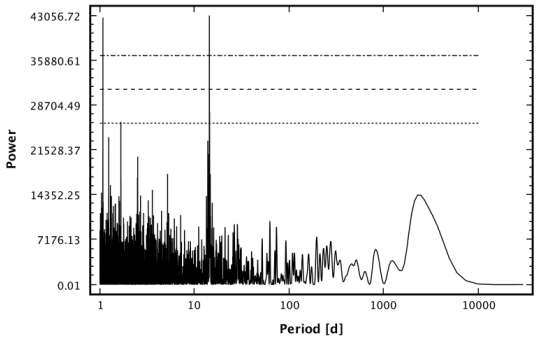

(5) GJ431

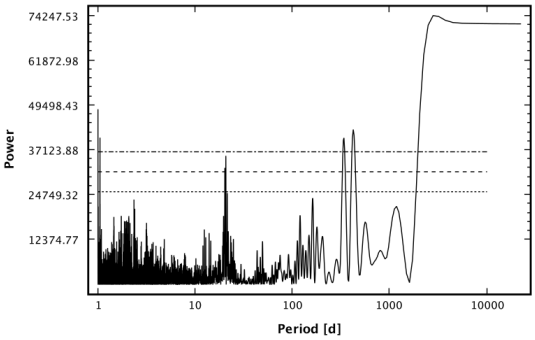

(6) GJ669A

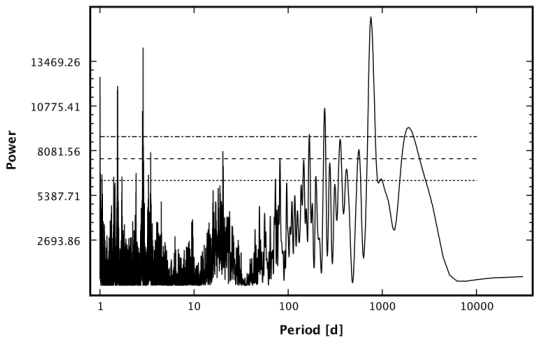

(7) GJ729

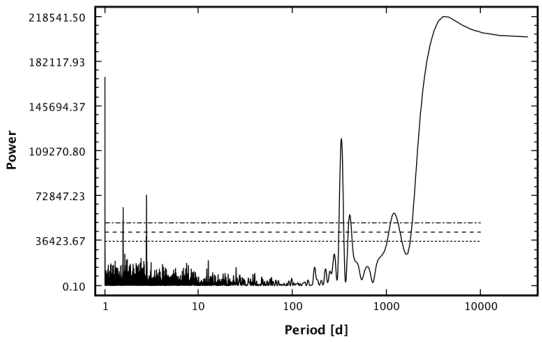

(8) GJ285

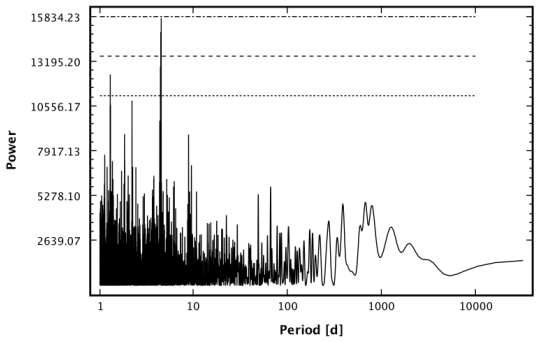

(9) GJ182

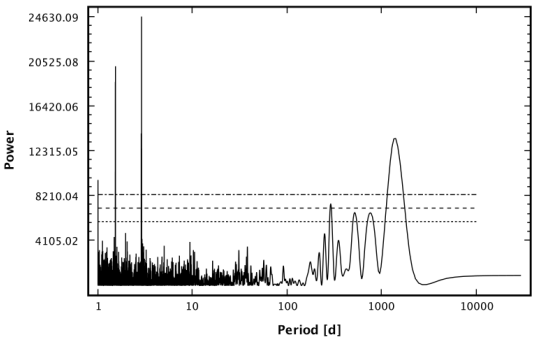

(10) GJ494

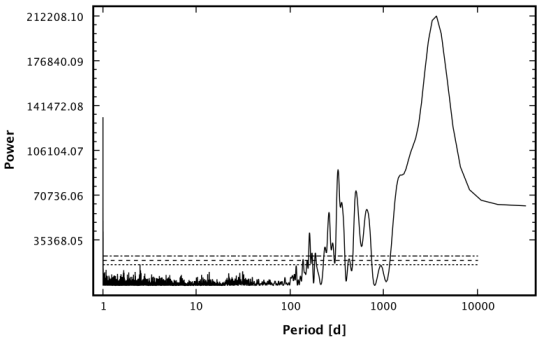

(11) GJ3331

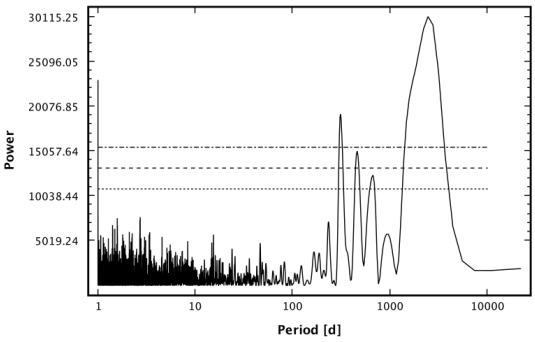

(12) GJ9520

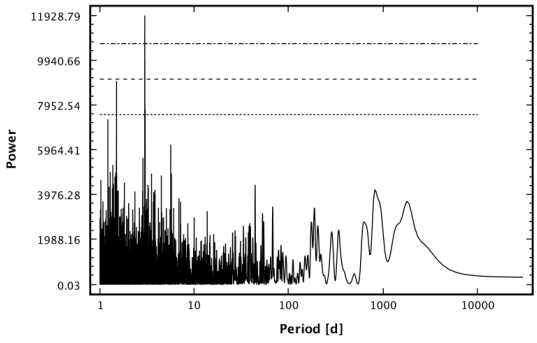

(13) GJ2036A

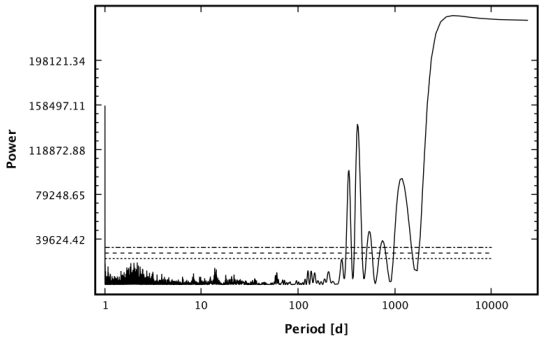

(14) GJ569A

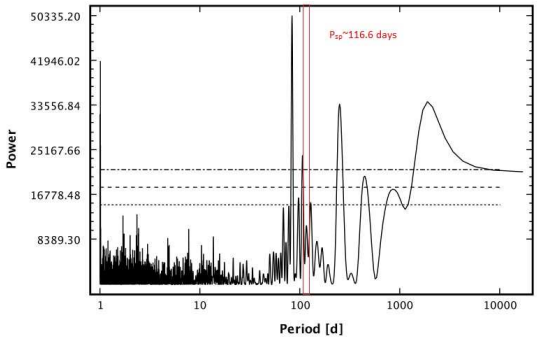

(15) GJ551

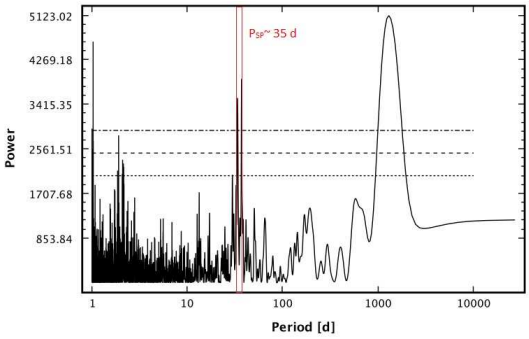

(16) GJ205

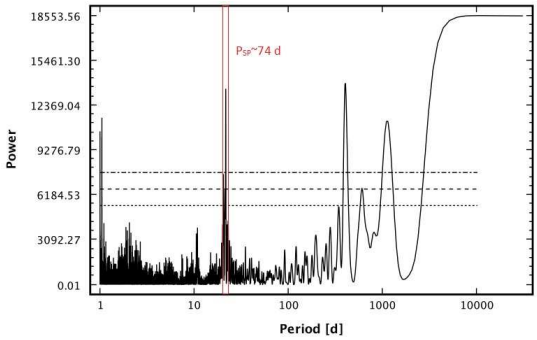

(17) GJ382

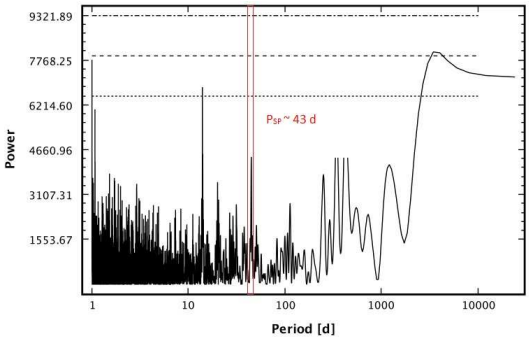

(18) GJ536

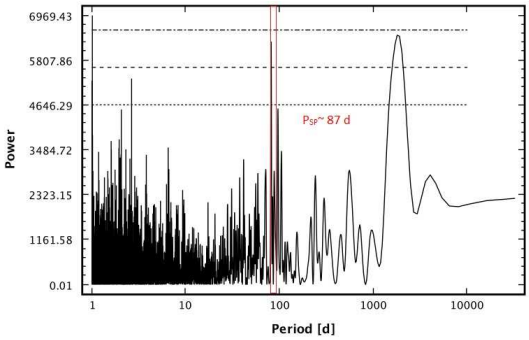

(19) GJ876

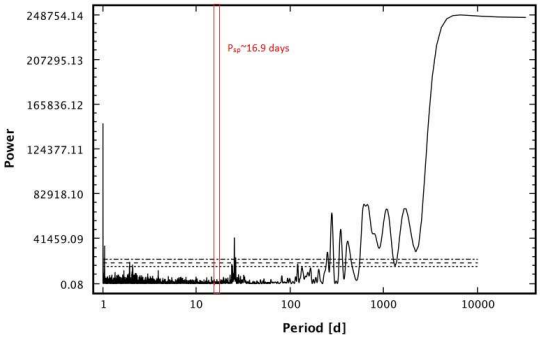

(20) GJ358

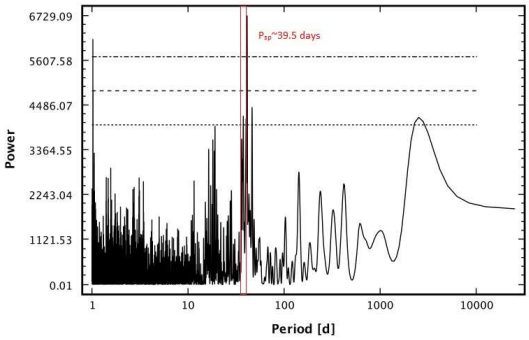

(21) GJ176

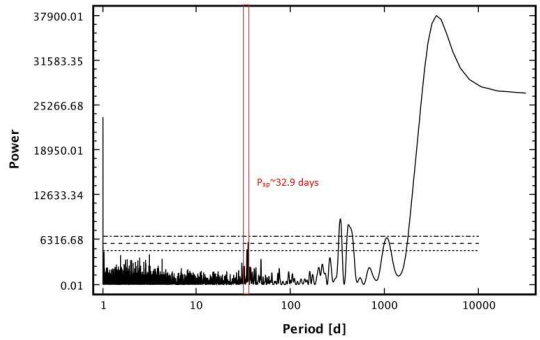

(22) GJ674

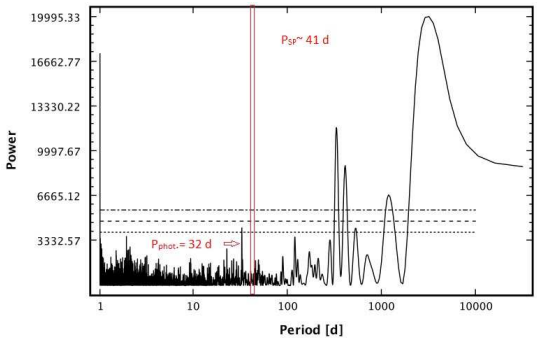

(23) GJ676A

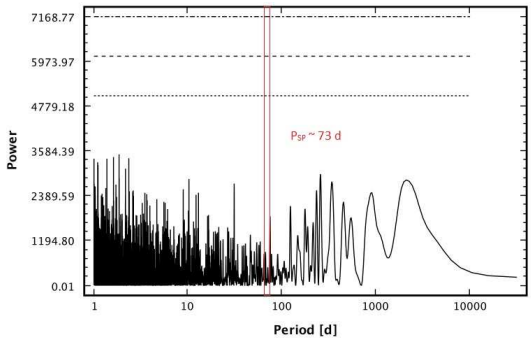

(24) GJ433

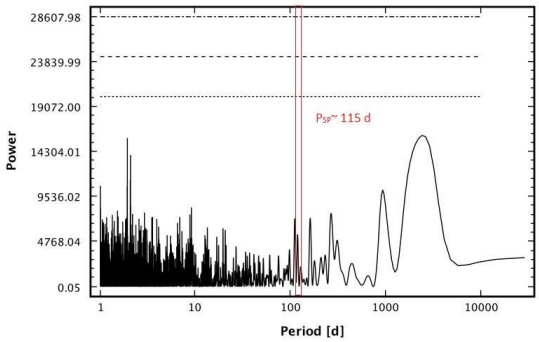

(25) GJ273

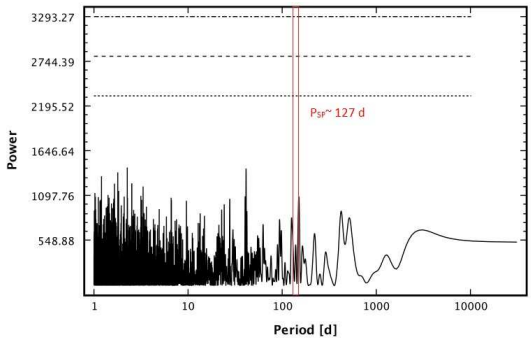

(26) GJ701

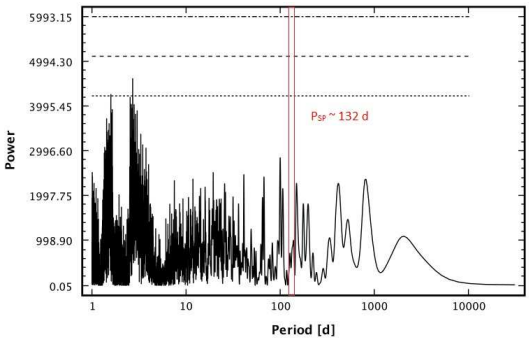

(27) GJ581

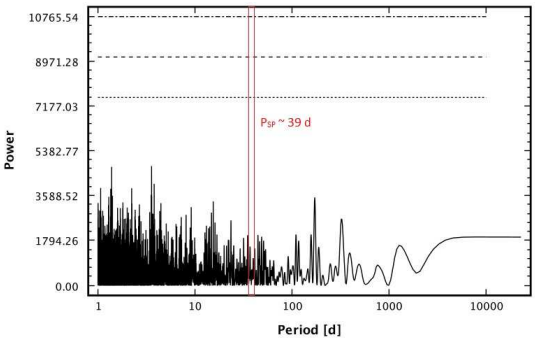

(28) GJ436

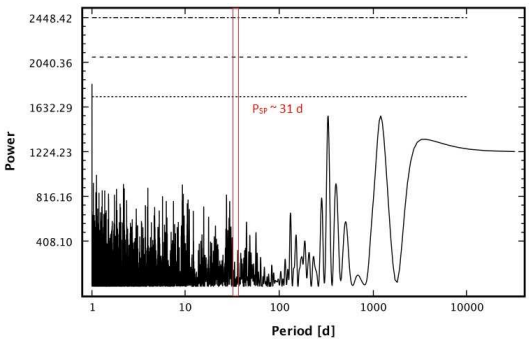

(29) GJ846

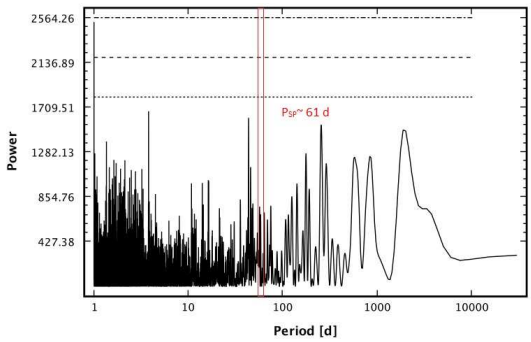

(30) GJ588

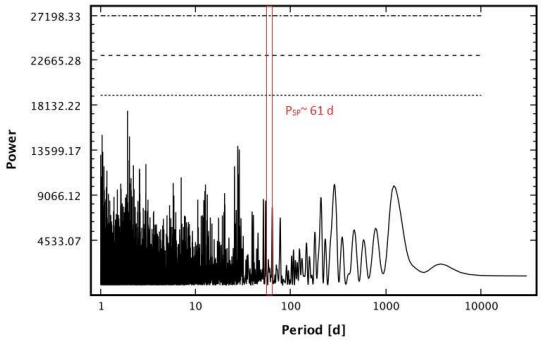

(31) GJ163

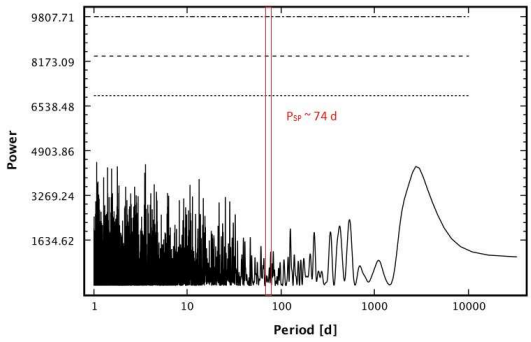

(32) GJ357

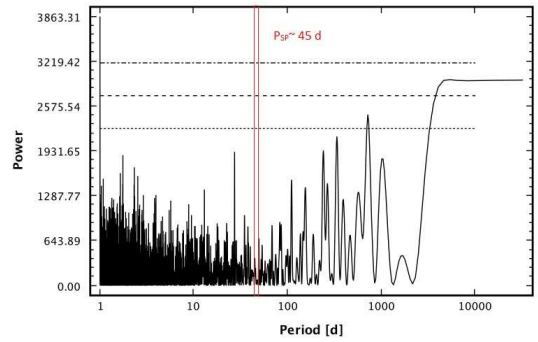

(33) GJ832

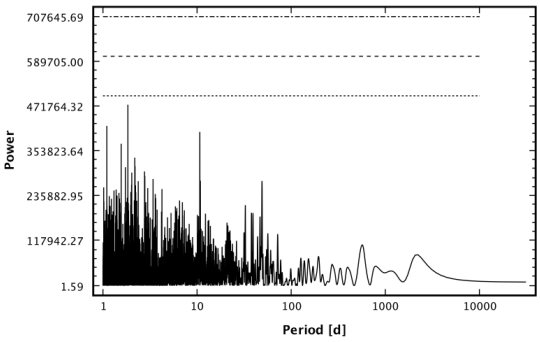

(34) GJ1057

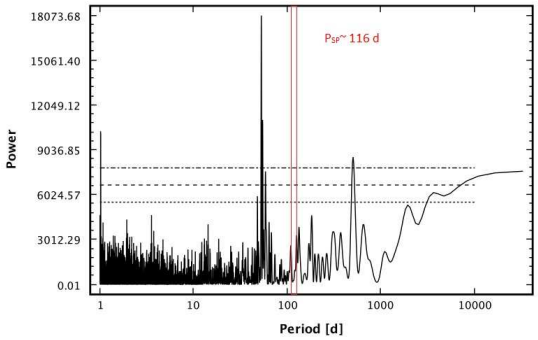

(35) GJ877

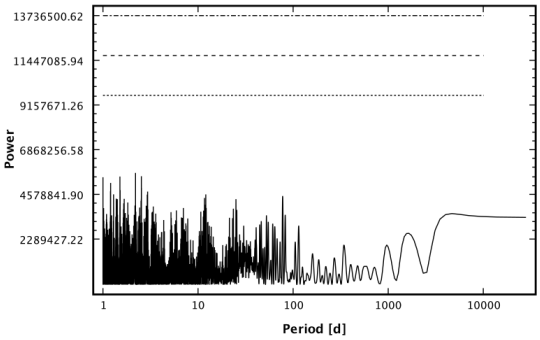

(36) GJ667C

Tables 4.2, 4.3, 4.4, 4.5 lists basic data for the targets and the results of the period search. There is a good agreement between our results and photometric rotation periods in the literature, especially with (Kiraga, 2007). The activity cycle or rotation period and their alias periods were identified by analysing periodograms, residual periodograms and window functions for each target.

Individual analysis of stars:

GJ 103 is a spectroscopic binary with spectral types M0 and V=8.85 mag, a strong periodogram peak was observed near 1.56 days, which agrees with 1.56 days found by (Kiraga, 2007). Peaks near to 2 days were discarded as aliases by rotation period and 341 days and 1621 days as yearly aliases caused by an activity cycle near 4600 days.

GJ 84 is a visual binary with the spectral type M2.5 and V =10 mag. The estimated rotation period identified was at 43.1 days. There are no other significant peaks in periodograms of this target (see periodogram 2 in Figure (4.1)).
GJ3367 is a rotationally variable star and the mean value rotation period 12.05 days, the same value as (Kiraga, 2007). No other significant variability in its periodogram was identified, see Figure 4.1

GJ375 is a spectroscopic binary with a period of 1.877 days, this is good agreement with (Kiraga, 2007). There is no other significant peak in periodogram.

GJ3331 and GJ9520 periodograms and periodograms of window function were analysed, we found that a peak near 1 day is caused by an alias.

GJ2036A is a pre-main sequence star with an estimated rotation period of 2.98 days. There is no other significant peak in periodogram. Although a peak was found 0.891 days at (Kiraga, 2007), it is considered to be an alias.

GJ205: besides having peak at 1292 days as its probable activity cycle, has two significant peaks, the first at 36.97 days which is possibly the differential rotation period of the rotation period at 33.54 days.

GJ551, GJ205, GJ382, GJ536, GJ876, GJ358, GJ176, GJ674, GJ676A, GJ433, GJ273, GJ701, GJ581, GJ436, GJ846, GJ588, GJ163, GJ357, GJ832, GJ877, GJ667C, these targets with spectroscopic rotation periods according to (Suárez Mascareño et al., 2015), we display in their periodograms the location of spectroscopic rotation periods and see how this agrees with what we found for photometric rotation periods.
We found, some agreement with 8 out of 21 targets having corresponding spectroscopic rotation periods. Figure (4.2) shows the spectroscopic periods compared with our photometric rotation period.

GJ551 has a detected photometric rotation period of 83.03 days, it is very close to the spectroscopic period of 82.6 days (Collins et al., 2016), with the same characteristics as GJ205, GJ382, GJ536, GJ176 and GJ674 . In the other four targets, a difference of a few days between our photometric period and spectroscopic periods was identified which we consider within the joint errors of these independently calculated periods. Though for some the differences were too large to claim consistency for GJ876 was ≈ 6 days, GJ358 was ≈ 9 days and GJ676A was ≈ 9 days. Nevertheless finding close values for rotation periods by different techniques indicate that these periods are correct.

GJ877: after we examined the apertures of this target, we found there is a small 12.19 arcsecond angular separation between target and its companion. Additionally, this companion has V-magnitude of 10.43, which is close to the brightness of the primary (10.3 mag). These two reasons did not allow us to resolve them, the interpretation of the joint signals for these targets in the periodogram is puzzling and beyond the scope of this work.

GJ667C, as with GJ877, due to its companion uncertainties for this target are very high (524 mmag) as shown in section(3.5.3), thus the ASAS photometric data presented here is not valid for our analysis.

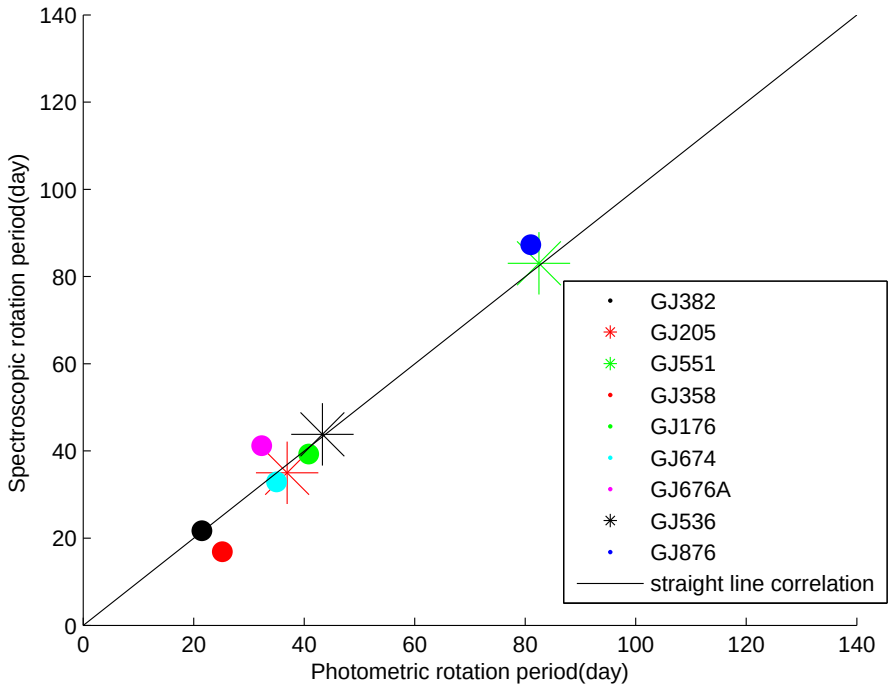

FIGURE 4.2: The consistency between spectroscopic and photometric rotation periods for targets which have both of them. They are GJ551, GJ205, GJ382, GJ536, GJ176 , GJ674, GJ876, GJ358 and GJ676A. we represent them by different coloured dots. The straight line shows the 1:1 relation.

Another group of stars shows no evidence of photometric rotation periods in their periodograms. The activity of most of these targets was checked by using CaIIH&K index as tracer as show in section (4.3). All of these stars was found to be inactive. Since photometric periods can be noticed in stars that have large brightness variations. The ASAS photometric data becomes difficult to apply to inactive stars to identify their rotation period and activity. The information of the rotation periods and activity of this kind of star depends on spectroscopic observations, as shown clearly in Table(4.8) and Figure (4.5).

In Figure (4.3), We compiled spectral type for M dwarfs and rotation periods in order to examine the rotation periods in the range of spectral types (M0-M6), we indicate M dwarfs that have spectroscopic rotation periods by circles, and use blue dots for photometric periods.

We show a possible sharp transition for rotation period values from 40 to 130 days occurs when moving from M1.5 to M2 spectral type. Likewise, we show most photometric rotation periods between ≈ 1 to ≈ 40 days. In general, photometric periods in our

sample tend to appear shorter than the spectroscopic periods.

In Figure(4.3), there is a range of rotation periods for every different spectral type. We did not have enough targets in each spectral type to achieve a statistically significant sample and there is no clear correlation between the spectral type of M dwarfs and their rotation periods beyond a weak trend for later spectral types to have longer periods.

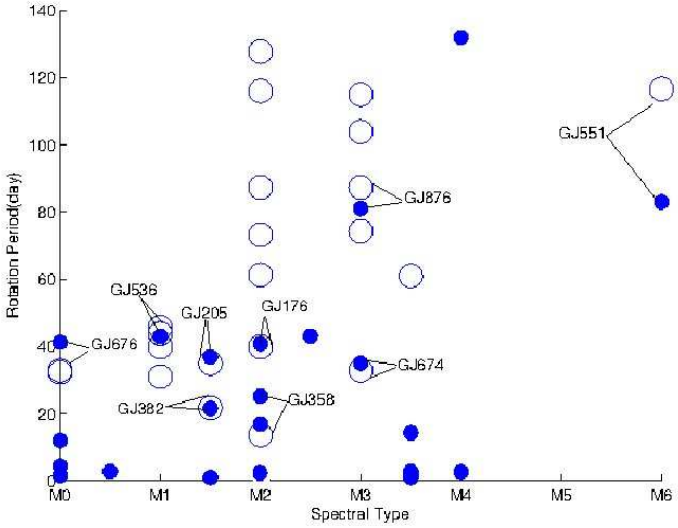

FIGURE 4.3: Distribution of rotation period depends on the spectral type. Circles represent the targets with spectroscopic rotation periods, while the blue points represent targets with photometric rotation periods

4.2 Matching between planetary orbital periods and stellar rotation periods

The identification of planetary signal is difficult when radial velocity variations induced by rotation period and activity coincide with the orbital period of the planet (Boisse et al., 2011).

In this section, the planetary orbital period's values for some of the candidate planets were compiled and matched with rotation periods values of their M dwarfs host to show the synchronization between them. The stellar activity signals, which appear at the stellar rotation period, can mimic the effect of a planet at these orbital periods or near of them. Therefore, it is important to understand how stellar rotation impacts the discovery of the exoplanets around their host stars.

The rotation period values for our sample range from 40 -132 days and spectral types are primarily from M0- M4. For example, GJ676A, has 4 detected planets. They are (b) at 1050 days (Forveille et al., 2011), (c) at 4400 days, (d)at 3.6 days, and (e) at 35.37 days (Anglada-Escudé and Tuomi, 2012). The latter planet(e), has an orbital period very close to our photometric rotation period(32.3 days). This makes us concerned that it could be caused by stellar rotation rather than a planet.

GJ876: There is a three candidate planets(d,c,b) at periods P_d=1.93 days, P_c=30 days and P_b=61.1 days. None of these are compatible with our rotation period of 81.19 days. We, therefore, suggest that these periods did not induce the rotation period of the star. For other stars, we did not find any matches between stellar rotation period and planet orbital period, see Table(4.6).

TABLE 4.6: Matching between our rotation periods and orbital periods of candidate exoplanets candidate exoplanets reported in the literature. The signal induced by stellar rotation could mimic the planetary signals at or near these orbital periods if the stellar rotation period of the star coincides with the orbital periods of the planets then it is rotation period and not planetary period. We indicate references of rotation periods by(1) for this work and (2) from (Suárez Mascareño et al., 2015). References of orbital periods(Ref.):(1)(Stevenson et al., 2012), (2)(Tuomi and Anglada-Escudé, 2013) (3)(Rivera et al., 2010), (4)(Delfosse et al., 2013), (5)(Anglada-Escudé et al., 2013), (6)(Forveille et al., 2011), (7)(Forveille et al., 2009), (8)(Anglada-Escudé et al., 2012), (9)(Wang and Ford, 2011), (10)(Forveille et al., 2011), (11)(Anglada-Escudé and Tuomi, 2012), (12)(Bailey et al., 2008) (13)(Wittenmyer et al., 2014)

Star	planet	P.orbital(d)	Ref.	P_{rot}
GJ436	b	$2.6438986 \pm 16 \times 10^{-6}$	(1)	39.9(2)
	c	$1.265862 \pm 8 \times 10^{-6}$		
GJ163	b	8.6313	(2)	61(2)
	c	25.662		
	d	567		
GJ876	d	$1.937781 \pm 24 \times 10^{-5}$	(3)	81.19(1)
	c	30.0880 ± 0.0091		
	b	61.1139 ± 0.0084		
GJ433	b	$7.3709 \pm 0.8 \times 10^{-4}$	(4)	73.2(2)
	c	3693 ± 253		
GJ581	b	$5.36865 \pm 0.9 \times 10^{-5}$	(6)	132 (2)
	e	$3.14945 \pm 17 \times 10^{-5}$		
	c	$12.9182 \pm 22 \times 10^{-4}$		
	d	66.64 ± 0.08		
GJ176	b	$8.7836 \pm 54 \times 10^{-4}$	(7)	40.87(1)
	c	4040.0 ± 0.11		
GJ674	b	4.6944 ± 0.00182	(9)	35(1)
GJ676A	b	1050 ± 1.2	(10)	32.3(1)
	c	4400	(11)	
	d	$3.600 \pm 8 \times 10^{-4}$	(11)	
	e	35.37 ± 0.07	(11)	
GJ832	b	3660	(12)	45.7(2)
	c	35.67 ± 0.15	(13)	

4.3 Examination of the relation between activity of M dwarf stars derived from Hα and CaII H&K measurements and rotation period

We collected measurements of stellar chromospheric activity $\log(L_{H\alpha}/L_{bol})$ from the literature and CaII H&K from HARPS data(High Accuracy Radial velocity Planet Searcher) as tracers of activity, this data was downloaded from the European Southern Observations archive. We used these measurements to study periodicities related to the rotation of our M dwarfs sample in the range of spectral type M0 to M6.

The lowest activity M dwarfs rotate slowly through active M dwarfs seem to rotate more rapidly with a rotation period ranging from a fraction of a day to several days (Pizzolato et al.,2003) and (Delfosse et al., 1998).

Table 4.7 and Figure 4.4 illustrate the relation between photometric periods found by this work for early-type M dwarfs (<M3) and their activity level measured using normalized $H\alpha$ luminosity from (Reiners et al., 2012). They take these measurements in the spectral range 6552-6572Å, where $\log(L_{H\alpha}/L_{bol})$= -4 meaning that magnetic fields are of the order of 2 kG or more. We could find values of $L_{H\alpha}/L_{bol}$ from (Reiners et al., 2012) for just seven targets, they are GJ182, GJ494, GJ3331A, GJ9520, GJ2036A, GJ358, GJ596A.

We see that low activity $\log(L_{H\alpha}/L_{bol}$ <-4.0) occurs at a relatively slow rotation period, GJ358 (P_{rot}=25.2 days) and GJ569A (P_{rot}=13.6 days). On the other side, the stars with $\log(L_{H\alpha}/L_{bol}$ >-4.0) are rapidly rotating and active.

TABLE 4.7: Activity of early-M stars with Hα measurements from (Reiners et al., 2012) and P_{rot} (rotation period) from this work. We put the normalized Hα luminosity; $\log(L_{H\alpha}/L_{bol})$ an indicator of activity for M dwarfs, versus the rotation period.

Target	Spectral type	$\log(L_{H\alpha}/L_{bol})$	P_{rot} (day)
GJ182	M0	-4.11	4.3
GJ494	M0.5	-3.80	2.8
GJ3331A	M1.5	-3.89	1.0003
GJ9520	M1.5	-3.92	1.0005
GJ2036A	M2	-3.45	2.9
GJ358	M2	-4.44	25.2
GJ569A	M2	-4.30	13.6

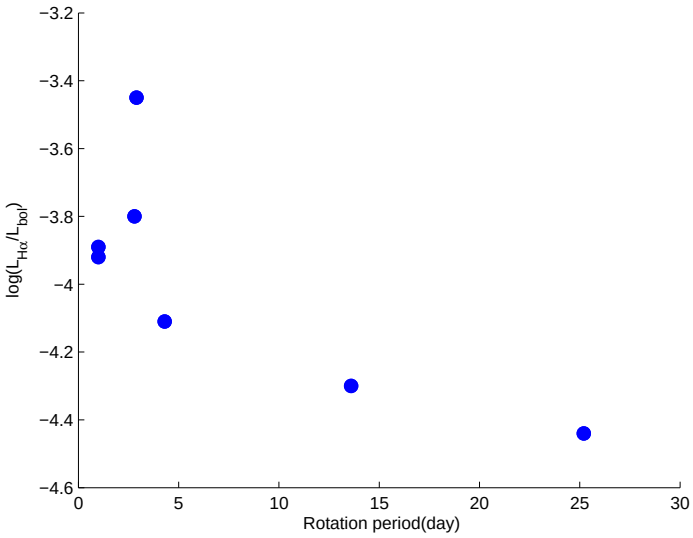

FIGURE 4.4: Normalized $H\alpha$ luminosity as a function of rotation period of active early-M dwarfs. There is increasing activity with decreasing rotation period.

Table 4.8 and Figure 4.5 depicts the relation between our photometric rotation periods in addition to spectroscopic periods for spectral type range (M0-M6) versus the average of activity level measured using the CaII H&K lines in the range of 3968.470Åto 3933.664Å, where CaII H&K lines measure chromospheric surface fluxes. We calculate the average value of activity from HARPS. The CaII H&K lines index measure the strength of the emission compared to a nearby continuum (Noyes et al., 1984).

We classified the dots in Figure 4.5 by different colours depending on how we measured the rotation periods, as follows:

1. Black dots represent stars that just have spectroscopic rotation periods and we did not find any evidence for the existence of photometric periods for them in our search with ASAS photometric data, They show the slowest rotators (31-127.8) days with lowest activity CaII H&K<1, with the exception of GJ701 (M2; early-type M dwarf) shown as more active than the rest of the black dots (2.33).

2. Green dots for five stars which have spectroscopic and photometric periods and we take the average value for each one of them. Four of them have rotation range of 20- 40 days with CaII H&K>1, except GJ876 which has an average rotation value of 84 days.

3. Red dots for stars which just have photometric periods from this work, they show the highest magnetic activity CaII H&K>1 with faster periods from 2.8 to 14 days, except for GJ551 (M6; late-type M dwarf), with the highest rotation in the sample (11.11 days) and slow rotation at 83 days.

   The green and red dots show an increase in activity strength with decreased rotation period, except GJ551. In contrast, black dots are consistent with having a close level of activity, except GJ701.

Figure (4.5A) indicates that all M dwarfs with periods shorter than 40 days show activity CaII H&K>1. In this range of activity and rotation, we can see a clear relation between them. In this situation with the CaII H&K index, seems certainly appropriate to study the relation between activity and rotation. (West et al., 2015) used $L_{H\alpha}$ as a tracer, and show that all M dwarfs (M1-M4) rotating faster than 26 days are magnetically active.

Also, we plot the Figure (4.5B) to show how the level of magnetic activity CaII H&K varies as a function of the rotation period. We take the natural logarithm both of them, we can see there is a clear decrease in the level of magnetic activity with increasing rotation period.

From Figures (4.5A&B) we can see, in the early-type M dwarf stars, the rapidly rotating stars are magnetically active, while slowly rotating stars are less active or inactive. But in the cases of GJ701 and GJ551, they have the slowest rotation but still show magnetic activity. Considerable studies have indicated that a broad portion of late- type M dwarfs as in the case of GJ551(M6) are seen to be active, possibly a result of their long activity lifetimes (Silvestri et al., 2005); (West et al., 2008). Also because there is a link

between rotation and age in all M dwarfs and the younger stars have a faster rotation and these targets can be considered as young stars(Kiraga, 2007) and (West et al., 2008).

We used Pearson's correlation coefficient (R) technique to measure the strength of linear relationship between CaII H&K indicators and stellar rotation, the value of R is between $(-1 \leqq R \leqq 1)$. When selecting the targets that have stellar rotation less than 40 days, we found strong negative correlation (-0.76). While, when we select all early M dwarfs, we found there is a moderate negative correlation(-0.63), the closer the value is to 1 or -1, the stronger the linear correlation.
We can say, there is a strong relationship between rotation and activity by CaII H&K for early M dwarfs that have stellar rotation less than 40 days. While there is moderate relation between rotation and activity for the range of stellar rotation of M dwarfs.

We can conclude that the early-type M dwarf stars show a decrease in their level of magnetic activity with increased rotation period. In contrast, the late-type M dwarf star (GJ551) is consistent with having a high level of activity at the longest rotation period.

It is worth noting that targets which have photometric rotation periods in Figure (4.5) are active CaII H&K>1 except GJ876, because these active stars have brightness variation produced by long lived spots on the stellar surface. Therefore photometric data are really useful for active stars.

TABLE 4.8: Activity of M dwarf stars with CaII H&K measurements from HARPS and photometric rotation period by this work and spectroscopy. We used CaII H&K as an indicator for the activity of M dwarfs, against the rotation period and spectral type (ST). The CaII H&K lines index measure the strength of the emission compared to nearby continuum (Noyes et al., 1984).

Target	ST	CaII H&K	$P_{\rm phot}$(day)	$P_{\rm sp}$(day)
GJ3367	M0	4.25	12.05	-
GJ182	M0	6.05	4.37	-
GJ494	M0.5	7.13	2.8	-
GJ382	M1.5	1.75	21.54	21.7
GJ205	M1.5	1.89	36.9	35
GJ846	M1	1.61	-	31
GJ436	M1	0.6	-	39.9
GJ358	M2	2.75	25.23	16.9
GJ433	M2	0.74	-	73.2
GJ588	M2	0.59	-	61.3
GJ674	M3	1.35	35.03	32.9
GJ832	M2	0.68	-	45.7
GJ701	M2	2.33	-	127.8
GJ877	M2	0.64	-	116
GJ357	M3	0.50	-	74.3
GJ876	M3	0.82	81.1	87.3
GJ273	M3	0.66	-	115
GJ163	M3.5	0.60	-	61
GJ431	M3.5	10.49	14.3	-
GJ581	M4	0.44	-	132
GJ551	M6	11.11	83.03	-

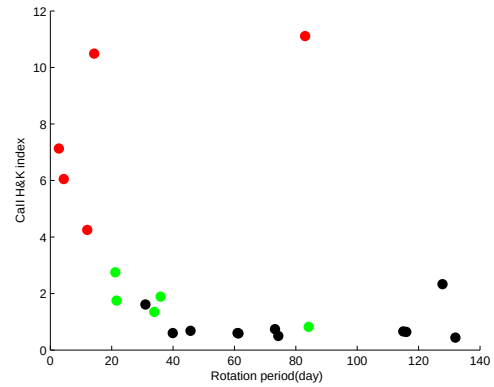

(A)

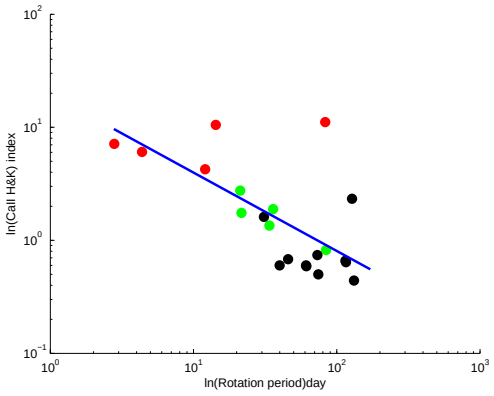

(B)

FIGURE 4.5: (A) CaII H&K index of activity stars as a function of rotation period, black dots represent targets which have just spectroscopic rotation period, green dots for targets have spectroscopic and photometric rotation periods (we take the average value for each one), red ones for targets just have photometric periods. (B) ln(CaII H&K) as a function of ln(rotation period) for the same targets in (A), we can see a clear decrease in the level of magnetic activity with increasing rotation period. The blue line is a linear least squares fitting.

Chapter 5

Conclusions

5.1 Period search

We used the ASAS-V database to search for significant signals in M dwarfs photometric data. We fin photometric data is a reliable source of data to analyse rotation periods of the M dwarfs stars which show large brightness variations, however, it is difficult to obtain rotation periods for photometric data where there is a low activity level.
Searching for the correct period is hampered by alias signals due to the daily observational gaps; in addition to there are also weather and instrumental problems, which introduce variability in the amplitude and phase of the periodogram. We interpreted all significant periods in each periodogram. The length of the identified rotation periods ranges from a day to more than 140 days.

We have compared our period measurements of photometric rotation periods with the photometric period determinations of (Kiraga, 2007) and others. In addition, we compare with the spectroscopic periods of (Suárez Mascareño et al., 2015). We found a good agreement with (Kiraga, 2007). However, this study only found agreement for 8 targets out of 20 targets where the spectroscopic rotation periods (Suárez Mascareño et al., 2015) are consistent with ASAS photometric periods. 23 out of 36 targets were identified to have a rotation period.

5.2 Identify the planetary signals

Stellar rotation periods frustrate the detection of exoplanets when using the radial velocity technique. Orbital periods of some candidate exoplanets from literature and rotation

periods for the M dwarf planet-host sample have been compiled in order to investigate any correlation between them.

If a period in a periodogram matches with a potential planetary period, that means it is probably a misidentification, see Table (4.6). Verifying that there is not a match of planetary orbital period with the stellar rotation period is really important confirming for the existence of an exoplanet.

Identifying stellar rotation activity plays a crucial role in the detection of exoplanets when using radial velocity technique, because they can mimic the effect of the orbital period of a planet around a hosted star.

For the GJ676A, it has 4 detected planets, (b, c, d, e). Our analysis has demonstrated that the latter planet (e) is compatible with our photometric rotation period (32.3 days), therefore, we suspect that it not a real planet but a sign of rotation. For other candidate planets, we did not find any evidence that they induced by stellar rotation

5.3 Rotation-activity relation

We have studied the relationship between the magnetic activity and rotation period in this work, using normalized $H\alpha$ luminosity and CaII HK as tracers of stellar chromospheric activity for 28 M dwarfs. The results of our analysis in this section are summarized as follows:

1. Rotation periods for seven M dwarfs (<M3) against $H\alpha$ illustrate strong evidence that all active stars ($L_{H\alpha}/L_{bol}$ >-4.0) are rapidly rotating, this agrees with the results of (Reiners et al., 2012).

2. Rotation periods for 19 out of 21 M dwarfs stars against CaII H&K, illustrate strong evidence that the level of magnetic active appears to drop with increasing rotation periods.

3. All M dwarfs with rotation periods shorter than 40 days with (CaII H&K>1), show strong evidence for a correlation between the activity-rotation relation for early-type stars (<M4). While (West et al., 2015) using $H\alpha$ as tracer, show that all M dwarfs (M1-M4) rotating faster than 26 days are magnetically active.

4. Rotation periods longer than 40 days with (CaII H&K<1) show a weak relationship, although there are two slowly rotating still active (GJ701, GJ551), which are likely to be younger stars (Kiraga, 2007), (West et al., 2015).

5. CaII H&K index is useful for M dwarfs stars with rotation periods shorter than 40 days with (CaII H&K>1).

   In general, we find a clear relationship between rotation and activity for our sample of early-type M dwarfs.

6. There is no clear correlation between rotation period and spectral type for M dwarfs. We could not find statistically significant results, because there are not enough stars in our sample in each spectral type bin. But we suggest there is a link between rotation and age in all M dwarfs. Therefore, we see short and long rotation in all range of early M dwarfs, that means, we can find younger M dwarfs in early and late-type, where they are rapidly rotating and likely to be active.

7. Photometric rotation periods are really useful to study rotation periods for active stars when CaII H&K>1.

Bibliography

Anglada-Escudé, G., Boss, A.P., Weinberger, A.J., et al., 2012. Astrometry and radial velocities of the planet Host M Dwarf GJ317: new trigonometric distance, metallicity, and upper limit to the mass of GJ317b. *The Astrophysical Journal*, 746:37.

Anglada-Escudé, G. and Tuomi, M., 2012. A planetary system with gas giants and super-Earths around the nearby M dwarf GJ 676A-Optimizing data analysis techniques for the detection of multi-planetary systems. *Astronomy & Astrophysics*, 548:58.

Anglada-Escudé, G., Tuomi, M., Gerlach, E., et al., 2013. A dynamically-packed planetary system around GJ 667C with three super-Earths in its habitable zone. *Astronomy & Astrophysics*, 556:126.

Bailey, J., Butler, R.P., Tinney, C., et al., 2008. A jupiter-like planet orbiting the nearby M dwarf GJ 832 Based on observations obtained at the Anglo-Australian Telescope, Siding Spring, Australia. *The Astronomical Journal*, 690:743.

Bochanski, J.J., Hawley, S.L., Covey, K.R., et al., 2010. The Luminosity and Mass Functions of Low-mass Stars in the Galactic Disk. II. The Field. *The Astronomical Journal*, 139:2679-2699.

Boisse, I., Bouchy, F., Hébrard, G., et al., 2011. Disentangling between stellar activity and planetary signals. *Astronomy & Astrophysics*, 528:4.

Browning, M.K., Basri, G., Marcy, G.W., et al., 2010. Rotation and magnetic activity in a sample of M-dwarfs. *The Astronomical Journal*, 139:504.

Cincotta, P.M., Mendez, M., and Nunez, J.A., 1995. Astronomical Time Series Analysis. I. A Search for Periodicity Using Information Entropy. *Astronomy & Astrophysics*, 449:231.

Collins, J.M., Jones, H.R.A., and Barnes, J.R., 2016. Calculations of periodicity from H{\alpha} profiles of Proxima Centauri. *Astronomy & Astrophysics*.

Covey, K.R., Hawley, S.L., Bochanski, J.J., et al., 2008. The Luminosity and Mass Functions of Low-Mass Stars in the Galactic Disk. I. The Calibration Region. *The Astronomical Journal*, 136:1778.

David, M., Hensberge, H., and Nitschelm, C., 2013. Detectability of micro-variables in the ASAS database. *Astronomy & Astrophysics*, 557:47.

Dawson, R.I. and Fabrycky, D.C., 2010. Radial velocity planets de-aliased: a new, short period for super-Earth 55 Cnc e. *Astronomy & Astrophysics*, 722:937.

Delfosse, X., Bonfils, X., Forveille, T., et al., 2013. The HARPS search for southern extra-solar planets-XXXIII. Super-Earths around the M-dwarf neighbors Gl 433 and Gl 667C. *Astronomy & Astrophysics*, 553:8.

Delfosse, X., Forveille, T., Beuzit, J.L., et al., 1999. New neighbours. I. 13 new companions to nearby M dwarfs. *Astronomy & Astrophysics*, 344:897.

Delfosse, X., Forveille, T., Perrier, C., et al., 1998. Rotation and chromospheric activity in field M dwarfs. *Astronomy & Astrophysics*, 331:581.

Forveille, T., Bonfils, X., Delfosse, X., et al., 2009. The HARPS search for southern extra-solar planets-XIV. Gl 176b, a super-Earth rather than a Neptune, and at a different period. *Astronomy & Astrophysics*, 493:645.

Forveille, T., Bonfils, X., Delfosse, X., et al., 2011. The HARPS search for southern extra-solar planets XXXII. Only 4 planets in the Gl 581 system. *Astronomy & Astrophysics*.

Horne, J.H. and Baliunas, S.L., 1986. A prescription for period analysis of unevenly sampled time series. *The Astrophysical Journal*, 302:757.

Houdebine, E.R., Mullan, D.J., Paletou, F., et al., 2016. Rotation-Activity Correlations in K and M Dwarfs. I. Stellar Parameters and Compilations of v sin i and P/sin i for a Large Sample of Late-K and M Dwarfs. *The Astrophysical Journal*, 822:97.

Huélamo, N., Figueira, P., Bonfils, X., et al., 2008. TW Hydrae: evidence of stellar spots instead of a Hot Jupiter. *Astronomy & Astrophysics*, 489:9.

Irwin, J., Berta, Z.K., Burke, C.J., et al., 2011. On the angular momentum evolution of fully convective stars: Rotation periods for field M-dwarfs from the MEarth transit survey. *The Astrophysical Journal*, 727:56.

Kiraga, M. & Stepien, K., 2007. Age-Rotation-Activity Relations for M Dwarf Stars. *Acta Astronomica*, 57:149.

Lomb, N.R., 1976. Least-squares frequency analysis of unequally spaced data. *Astronomy & Astrophysics*, 39:447.

Lovis, C. and Fischer, D., 2010. *Radial Velocity Techniques for Exoplanets*, pages 27–53.

Mayor, M. & Queloz, D., 1995. A Jupiter-mass companion to a solar-type star. *Nature*, 378:355.

Meschiari, S., Wolf, A.S., Rivera, E., et al., 2009. Systemic: A testbed for characterizing the detection of extrasolar planets. I. The Systemic Console Package. *Publications of the Astronomical Society of the Pacific*, 121:1016.

Nelson, B.E., Robertson, P.M., Payne, M.J., et al., 2016. An empirically derived three-dimensional Laplace resonance in the Gliese 876 planetary system. *Monthly Notices of the Royal Astronomical Society*, 455:2484.

North, G. and James, N., 2004. *Observing Variable Stars, Novae, and Supernovae.*

Noyes, R.W., Hartmann, L.W., Baliunas, S.L., et al., 1984. Rotation, convection, and magnetic activity in lower main-sequence stars. *The Astronomical Journal*, 279:763.

Omiya, M., Sato, B., Harakawa, H., et al., 2012. Search for Low-Mass Planets Around Late-M Dwarfs Using IRD. *Proceedings of the International Astronomical Union*, 8:201.

Pallavicini, R., Golub, L., Rosner, R., et al., 1981. Relations among stellar X-ray emission observed from Einstein, stellar rotation and bolometric luminosity. *The Astrophysical Journal*, 248:279.

Philip, A.G.D., 1985. Book-Review - Stellar Radial Velocities. *Sky and Telescope*, 70:336.

Pizzolato, N., Maggio, A., Micela, G., et al., 2003. The stellar activity-rotation relationship revisited: Dependence of saturated and non-saturated X-ray emission regimes on stellar mass for late-type dwarfs. *Astronomy & Astrophysics*, 397:147.

Pojmanski, G., 2002. The All Sky Automated Survey. Catalog of Variable Stars. I. 0 h-6 hQuarter of the Southern Hemisphere. *Acta Astronomica*, 52:397.

Pojmański, G., 2004. The all sky automated survey. *Astronomische Nachrichten*, 325:553.

Reiners, A., Joshi, N., and Goldman, B., 2012. A Catalog of Rotation and Activity in Early-M Stars. *The Astronomical Journal*, 143:93.

Rivera, E.J., Laughlin, G., Butler, R.P., et al., 2010. The Lick-Carnegie Exoplanet Survey: a Uranus-Mass Fourth Planet for GJ 876 in an Extrasolar Laplace Configuration. *The Astrophysical Journal*, 719:890.

Robertson, P., Endl, M., Henry, G.W., et al., 2015. Stellar Activity and its Implications for Exoplanet Detection on GJ 176. *The Astrophysical Journal*, 801:79.

Robertson, P., Mahadevan, S., Endl, M., et al., 2014. Stellar activity masquerading as planets in the habitable zone of the M dwarf Gliese 581. *Science*, 345:440.

Saar, S.H. and Donahue, R.A., 1997. Activity-related radial velocity variation in cool stars. *The Astrophysical Journal*, 485:319.

Scargle, J.D., 1982. Studies in astronomical time series analysis. II - Statistical aspects of spectral analysis of unevenly spaced data. *Astronomy & Astrophysics*, 263:835.

Schulman, E. and Cox, C.V., 1997. Misconceptions about astronomical magnitudes. *Astronomy & Astrophysics*, 65:1003.

Silvestri, N.M., Hawley, S.L., and Oswalt, T.D., 2005. The Chromospheric Activity and Ages of M Dwarf Stars in Wide Binary Systems. *The Astronomical Journal*, 129:2428.

Stevenson, K.B., Harrington, J., Lust, N.B., et al., 2012. Two nearby sub-Earth-sized exoplanet candidates in the GJ 436 system. *The Astrophysical Journal*, 755:9.

Sturrock, P.A. and Scargle, J.D., 2010. False-alarm Probability in Relation to Over-sampled Power Spectra, with Application to Super-Kamiokande Solar Neutrino Data. *The Astrophysical Journal*, 718:527.

Suárez Mascareño, A., Rebolo, R., González Hernández, J.I., et al., 2015. Rotation periods of late-type dwarf stars from time series high-resolution spectroscopy of chromospheric indicators. *Monthly Notices of the Royal Astronomical Society*, 452:2745.

Swan, P.R., 1982. Discrete Fourier Transforms of Nonuniformly Spaced Data. *The Astronomical Journal*, 87:1608.

Tuomi, M. and Anglada-Escudé, G., 2013. Up to four planets around the M dwarf GJ 163-Sensitivity of Bayesian planet detection criteria to prior choice. *Astronomy & Astrophysics*, 556:111.

Wang, J. and Ford, E.B., 2011. On the eccentricity distribution of short-period single-planet systems. *Monthly Notices of the Royal Astronomical Society*, 418:1822.

West, A.A., Hawley, S.L., Bochanski, J.J., et al., 2008. Constraining the age-activity relation for cool stars: the Sloan Digital Sky Survey Data Release 5 low-mass star spectroscopic sample. *The Astronomical Journal*, 135:785.

West, A.A., Weisenburger, K.L., Irwin, J., et al., 2015. An Activity-Rotation Relationship and Kinematic Analysis of Nearby Mid-to-Late-Type M Dwarfs. *The Astrophysical Journal*, 812:3.

Wittenmyer, R.A., Tuomi, M., Butler, R., et al., 2014. GJ 832C: A Super-Earth in the Habitable Zone. *The Astrophysical Journal*, 791:114.